Progress in Oceanography 213 (2023) 103018

Contents lists available at ScienceDirect

Progress in Oceanography

journal homepage: www.elsevier.com/locate/pocean

Earlier sea-ice melt extends the oligotrophic summer period in the Barents Sea with low algal biomass and associated low vertical flux

Doreen Kohlbach [a,*], Lucie Goraguer [a], Yasemin V. Bodur [b], Oliver Müller [c], Martí Amargant-Arumí [b], Katalin Blix [d,e], Gunnar Bratbak [c], Melissa Chierici [f,g], Anna Maria Dąbrowska [h], Ulrike Dietrich [b], Bente Edvardsen [i], Laura M. García [a,b], Rolf Gradinger [b], Haakon Hop [a], Elizabeth Jones [f], Øyvind Lundesgaard [a], Lasse M. Olsen [c], Marit Reigstad [b], Karoline Saubrekka [i], Agnieszka Tatarek [h], Józef Maria Wiktor [h], Anette Wold [a], Philipp Assmy [a]

[a] Norwegian Polar Institute, Fram Centre, Tromsø, Norway
[b] Department for Arctic and Marine Biology, UiT – The Arctic University of Norway, Tromsø, Norway
[c] Department of Biological Sciences, University of Bergen, Bergen, Norway
[d] Department of Physics and Technology, UiT – The Arctic University of Norway, Tromsø, Norway
[e] Balaton Limnological Research Institute, Tihany, Hungary
[f] Institute of Marine Research, Tromsø, Norway
[g] Department of Arctic Geophysics, University Centre in Svalbard, Longyearbyen, Svalbard, Norway
[h] Department of Marine Ecology, Institute of Oceanology Polish Academy of Sciences, Sopot, Poland
[i] Department of Biosciences, University of Oslo, Oslo, Norway

ARTICLE INFO

Keywords:
Planktonic protist communities
Vertical flux
Barents Sea
Climate change
Sea ice

ABSTRACT

The decrease in Arctic sea-ice extent and thickness as a result of global warming will impact the timing, duration, magnitude and composition of phytoplankton production with cascading effects on Arctic marine food-webs and biogeochemical cycles. Here, we elucidate the environmental drivers shaping the composition, abundance, biomass, trophic state and vertical flux of protists (unicellular eukaryotes), including phytoplankton, in the Barents Sea in late August 2018 and 2019. The two years were characterized by contrasting sea-ice conditions. In August 2018, the sea-ice edge had retreated well beyond the shelf break into the Nansen Basin (>82°N), while in 2019, extensive areas of the northwestern Barents Sea shelf (>79°N) were still ice-covered. These contrasting sea-ice conditions resulted in marked interannual differences in the pelagic protist community structure in this area. In August 2018, the protist community was in a post-bloom stage of seasonal succession characterized by oligotrophic surface waters and dominance of small-sized phytoplankton and heterotrophic protists (predominantly flagellates and ciliates) at most stations. In 2019, a higher contribution of autotrophs and large-celled phytoplankton, particularly diatoms, to total protist biomass compared to 2018 was reflected in higher chlorophyll *a* concentrations and suggested that the protist community was still in a late bloom stage at some stations. It is noteworthy that particularly diatoms contributed a considerably higher proportion to the protist biomass at the ice-covered stations in both years compared to the open-water stations. This pattern was also evident in the higher vertical protist biomass flux in 2019, dominated by dinoflagellates and diatoms, compared to 2018. Our results suggest that the predicted transition toward an ice-free Barents Sea will lengthen the oligotrophic summer period with low algal biomass and associated low vertical flux.

1. Introduction

Ecosystem structures, ecological interactions and dynamics in the Barents Sea are strongly driven by water-mass characteristics and seasonality in this high-latitude environment. Separated by the Polar Front (Parsons et al., 1996), the northern (Arctic) part of the Barents Sea with

* Corresponding author.
E-mail address: Doreen.kohlbach@npolar.no (D. Kohlbach).

https://doi.org/10.1016/j.pocean.2023.103018

Available online 21 March 2023

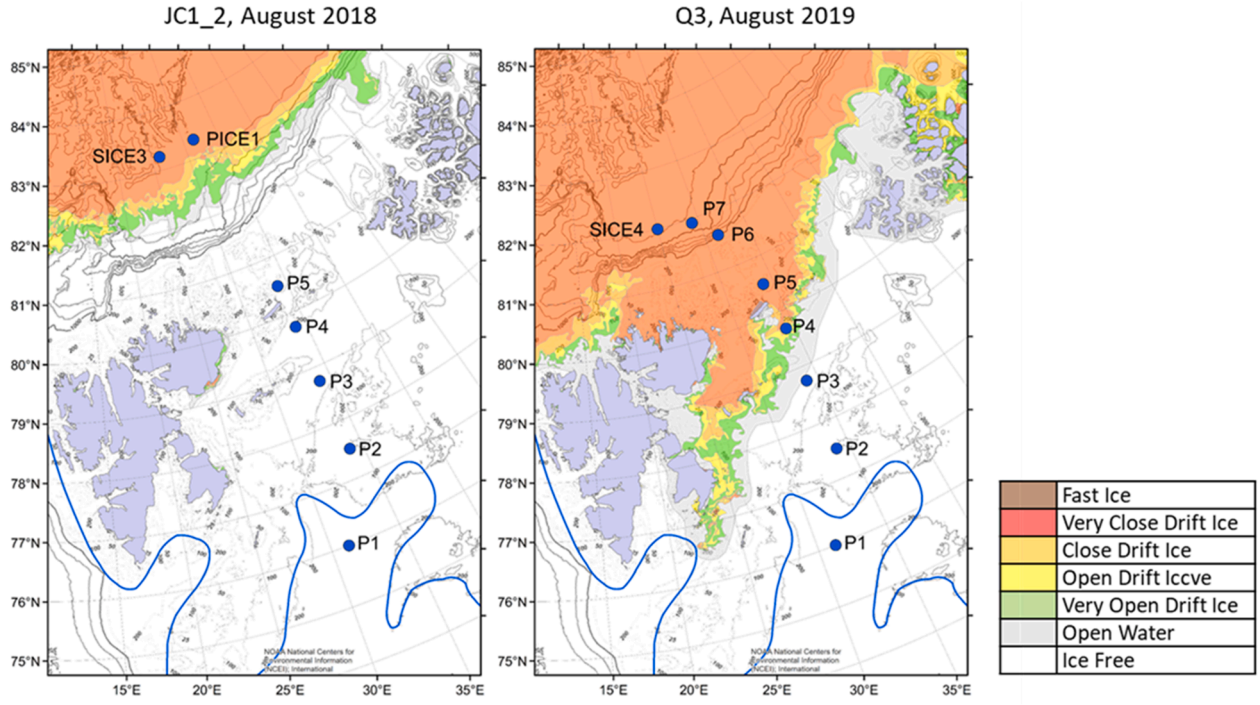

Fig. 1. Sampling station locations and sea-ice conditions in the northwestern Barents Sea during the Nansen Legacy cruises JC1_2 in August 2018 and Q3 in August 2019. The blue line indicates the position of the Polar Front (as indicated by the 0 °C surface isotherm) and was provided by the Institute of Marine Research. Ice data are from 15 August 2018 and 15 August 2019 and were provided by the Norwegian Ice Service - MET Norway.

cold and low-salinity Arctic water entering from the northeast is typically ice-covered in winter (Smedsrud et al., 2013), while the southern (subarctic) part remains ice-free for the majority of the year due to the inflow of warm, saline and nutrient-rich Atlantic water masses (Loeng, 1991; Loeng et al., 1997; Wassmann et al., 2006; Loeng and Drinkwater, 2007; Hunt et al., 2013). The Barents Sea is a highly productive shelf sea, particularly the subarctic part, supporting large zooplankton and commercial fish stocks, which in turn represent important prey for seals, whales, and seabirds (Wassmann et al., 2006; Loeng and Drinkwater, 2007; Sakshaug et al., 2009).

Apparent from the large-scale environmental changes observed over the past decades in the study region, the Barents Sea is particularly sensitive to climate warming (Skagseth et al., 2020; Isaksen et al., 2022; Smedsrud et al., 2022). Increasing volumes of inflowing warm Atlantic water masses (Oziel et al., 2016; Lind et al., 2018) lead to the continuous decrease in sea-ice extent and cause thinning of the ice cover during all seasons (Årthun et al., 2012, 2019, 2021; Onarheim and Årthun, 2017). While gross pelagic primary production is predicted to increase with declining sea-ice cover and consequently longer open-water seasons (Ellingsen et al., 2008; Drinkwater, 2011; Arrigo and van Dijken, 2015), increasing stratification of the surface water column in summer can amplify nutrient limitation reducing phytoplankton growth (Tremblay et al., 2009; Slagstad et al., 2015) and favour regenerated production and communities (Tremblay et al., 2015). Additionally, rising atmospheric CO_2 levels are resulting in acidification of the ocean, which is expected to affect calcifying organisms negatively (Kroeker et al., 2013; Skogen et al., 2014).

Superimposed on climate-change trends, multidecadal and interannual variations in ocean heat transport caused by large-scale climatic forcing (Vinje, 2001; Smedsrud et al., 2013, 2022; Oziel et al., 2016) have a marked impact on primary and secondary production, and subsequently ecosystem dynamics in the Barents Sea (Reigstad et al., 2002; Dalpadado et al., 2014; Ingvaldsen et al., 2021). Extended periods of open water, as the direct result of sea-ice loss caused by warming, but also interannual variability in sea-ice extent will impact the timing and magnitude of the primary production as well as the composition of phytoplankton communities in the Barents Sea (Neeley et al., 2018; Dalpadado et al., 2020; Dong et al., 2020). Earlier ice break-up and melt lead to earlier phytoplankton blooms in the northern Barents Sea and a longer open-water season to an increase in pelagic annual net primary productivity (Kahru et al., 2016; Dalpadado et al., 2020). However, the length of the highly productive period has not increased, which is likely the result of nutrient depletion as the season progresses (Kahru et al., 2016; Lewis et al., 2019). This will have consequences for vertical flux and the energy transfer to the seafloor during the extended low-productive summer season.

Atlantic and Arctic water masses in the Barents Sea, characterised by different properties and varying sea-ice conditions, host distinctly different phytoplankton communities (Owrid et al., 2000; Metfies et al., 2016; Downes et al., 2021). The composition of marine protist plankton communities in the Barents Sea changes seasonally. In spring, diatoms often dominate algal biomass (von Quillfeldt, 2000; Degerlund and Eilertsen, 2010; Vodopyanova et al., 2020), while after the spring diatom bloom, motile taxa, such as flagellates belonging to the prymnesiophytes, are a prominent component of the phytoplankton community in the subarctic part in this period (Giraudeau et al., 2016; Silkin et al., 2020). Also, other flagellates and heterotrophic protists reach their peak (Ratkova and Wassmann, 2002). Physical factors, such as the presence of sea ice, temperature and salinity of seawater, light conditions and mixed layer depth, chemical factors, including nutrient availability as well as biological factors, such as top-down control by pathogens, parasites and grazers have decisive impacts on the composition of phytoplankton and protist communities (Neeley et al., 2018; Sugie et al., 2020). In addition, the fact that the spring bloom is usually dominated by a few diatom species belonging to the genera *Thalassiosira* and *Chaetoceros* and the haptophyte *Phaeocystis pouchetii* points to life-cycle strategies, including defence against grazers, that have evolved to optimize resource uptake after the end of winter (Hegseth et al., 2019; Assmy et al., 2023).

Climate-driven changes in algal communities at the base of the

Table 1
Stations in the northwestern Barents Sea sampled for environmental variables (sections 2.3, 2.4, 3.2 and 3.3), protist community composition (microscopy; sections 2.5.1 and 3.4), pico- and nanoplankton (flow cytometry; sections 2.5.2 and 3.5) and protist vertical flux (sections 2.5.3 and 3.6) in August 2018 and 2019.

2018						2019					
Station #	Date of sampling	Latitude °N	Longitude °E	Bottom depth (m)	Standard sampling depths (m)*	Station #	Date of sampling	Latitude (°N)	Longitude (°E)	Bottom depth (m)	Standard sampling depths (m)*
P1[+]	08/08	75.997	31.229	325	5, 10, 20, 30, 40, 60, 90	P1[+]	08/08	76.000	31.219	325	5, 10, 30, 45, 60, 90
P2[+]	10/08	77.502	33.996	192	5, 10, 20, 30, 40, 60, 90	P2	12/08	77.501	33.987	186	10, 30, 50, 60
P3	12/08	78.751	33.998	305	5, 10, 20, 30, 40, 60, 90	P3	13/08	78.749	34.001	307	10, 30, 60, 90
P4[+]	14/08	79.749	34.001	335	5, 10, 20, 30, 40, 60, 90	P4[+]	14/08	79.693	34.230	353	10, 30
P5	15/08	80.501	34.006	163	5, 20, 30, 40, 60, 90	P5[+]	15/08	80.497	33.989	163	20, 30, 90
PICE1[+]	17/08 & 18/08	83.332/ 83.349	31.540/ 31.577	3930	5, 10, 30, 40, 60, 90	P6[+]	18/08	81.585	31.519	1100	10, 30, 90
SICE3	20/08	83.226	26.125	3911	5, 10, 20, 30	P7[+]	21/08	81.926	29.139	3300	15, 30, 60, 90
						SICE4	24/08	81.978	24.473	3600	10, 20, 30, 60, 90

*Deviations are noted in respective sections.
[+] Sampling stations for vertical particle flux.

pelagic food web will have cascading effects on the entire Arctic marine ecosystem (Hays et al., 2005; Post et al., 2013; Thingstad, 2020). Assessing qualitative and quantitative changes in protist plankton (especially primary producers) under contrasting environmental scenarios is therefore essential for developing a better understanding of ecosystem characteristics in the decades to come (Acevedo-Trejos et al., 2014; Lyon and Mock, 2014; Barton et al., 2016). While some microalgae seem to be able to acclimate to their changing habitat (Pančić et al., 2015; Rivero-Calle et al., 2015; Hoppe et al., 2018), others are likely to be impacted negatively (Hare et al., 2007; Coello-Camba et al., 2014; Kvernvik et al., 2018). As a result of a prolonged open-water season, warming waters, increasing CO_2 concentrations and reduced nutrient availability, the trend toward small-sized algae (picoplankton) has been reported for different parts of the Arctic Ocean (Li et al., 2009; Morán et al., 2010; Coello-Camba et al., 2014; Zhang et al., 2015; Sugie et al., 2020), where they succeed over large-sized diatoms (Marinov et al., 2010).

In this study, we assessed and compared the composition of planktonic protist communities and their vertical flux along a south-north transect in the northwestern Barents Sea during two years with contrasting sea-ice conditions. We related their taxonomic compositions and size structures, from pico- to microplankton, to environmental conditions (sea-ice cover, temperature, salinity, nutrients) in order to reveal the drivers of interannual variability in biomass, abundance and diversity of the Barents Sea microbial food web. The contrasting two years with different ice conditions provided a unique opportunity to test the hypothesis that earlier ice melt would lead to an earlier spring bloom and an extended oligotrophic summer season dominated by flagellates.

2. Material and methods

2.1. Sampling campaigns

Seawater samples were collected in August of two consecutive years (2018, 2019) within the framework of the Norwegian Nansen Legacy project (arvenetternansen.com). Both sampling campaigns were conducted onboard RV *Kronprins Haakon* during a similar summer period (2018: 6 to 23 August, seven stations, joint cruise JC1_2; 2019: 5 to 27 August, eight stations, seasonal cruise Q3). The northward transects covered areas from 76°N to 83°N in the northwestern Barents Sea (Fig. 1, Table 1). Details on individual sampling procedures can be found in the project sampling protocols (https://doi.org/10.7557/nlrs.5719).

2.2. Sea-ice conditions

Sea-ice conditions along the entire cruise track were assessed using the standardized IceWatch ASSIST protocol (https://icewatch.met.no/data_guide). Briefly, visual observations conducted regularly provided information on ice concentration, primary ice type, snow depth as well as melt-pond coverage. The entire data for both expeditions is available online (https://icewatch.met.no/) and only ice conditions within the vicinity of our biological stations are reported in this study (Table A.1).

2.3. Temperature, salinity and inorganic nutrients

Water-column temperature and salinity measurements were obtained using a conductivity-temperature-depth (CTD) sensor (Sea-Bird SBE 911plus) mounted onto a rosette equipped with 24 10*L*-Niskin bottles. All CTD data can be found in Ingvaldsen (2022) and Reigstad (2022). Seawater samples for the determination of nitrate [NO_3^-], phosphate [PO_4^{3-}] and silicic acid [$Si(OH)_4$] were drawn from the Niskin bottles into 20 mL pre-rinsed plastic HDPE vials and were preserved with 250 µL chloroform and stored in the dark at 4 °C. Post-cruise analysis was performed using a Flow Solution IV analyzer (O.I. Analytical, USA) following standard procedures (Grasshoff et al., 2009) at the Institute of Marine Research, Bergen, Norway. The analyser was calibrated by routine measurements of reference seawater obtained from Ocean Scientific International Ltd., UK. Detection limits were 0.5 µmol L^{-1} for [NO_3^-], 0.06 µmol L^{-1} for [PO_4^{3-}] and 0.7 µmol L^{-1} [$Si(OH)_4$], respectively. All nutrient data can be found in Chierici et al. (2021a,b).

Photosynthetically active radiation intensity (µmol m^{-2} s^{-1}) was retrieved from a Biospherical Licor Chelsea sensor mounted onto the rosette. The direct output of the sensor was used at all stations in 2018, and the P1 station in 2019. At stations P2-SICE4 in 2019, the rosette was deployed through the vessel's moonpool and the shadow of the vessel impacted the light measurements down to 25–30 m. For those stations, a Beer-Lambert curve was fitted on the data beyond this depth in order to model what the surface irradiance would have been. For the sea ice-covered stations, a light transmittance of 4 % under summer first-year ice with <10 cm of snow covered was assumed (Nicolaus et al., 2012) in order to estimate the irradiance incident on the sea-ice surface. An average between the above numbers, using the ice-cover proportion as weighing factor, was calculated to obtain a representative surface irradiance at each station.

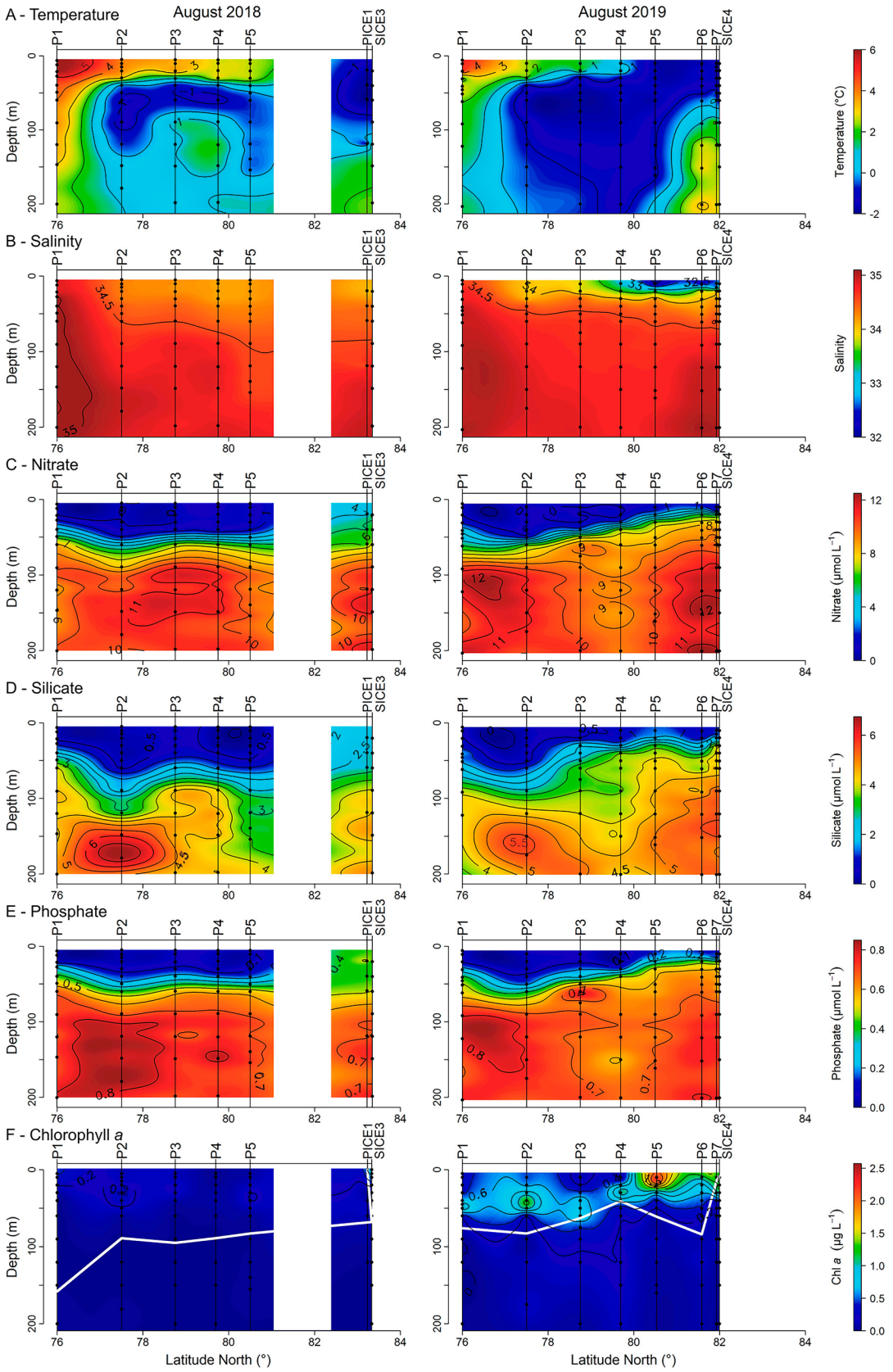

Fig. 2. A) Temperature (°C), B) salinity, concentrations of C) nitrate (µmol L^{-1}), D) silicate (µmol L^{-1}), E) phosphate (µmol L^{-1}) and F) Chlorophyll (chl) *a* concentration (µg L^{-1}) including the euphotic zone depth (white line) represented by the depth where photosynthetic available radiation (PAR) is 1% of PAR incident at the ocean surface, along the sampling transects in the northwestern Barents Sea in August 2018 (left panels) and August 2019 (right panels). The sampled depths (black dots) are plotted along the station (black line).

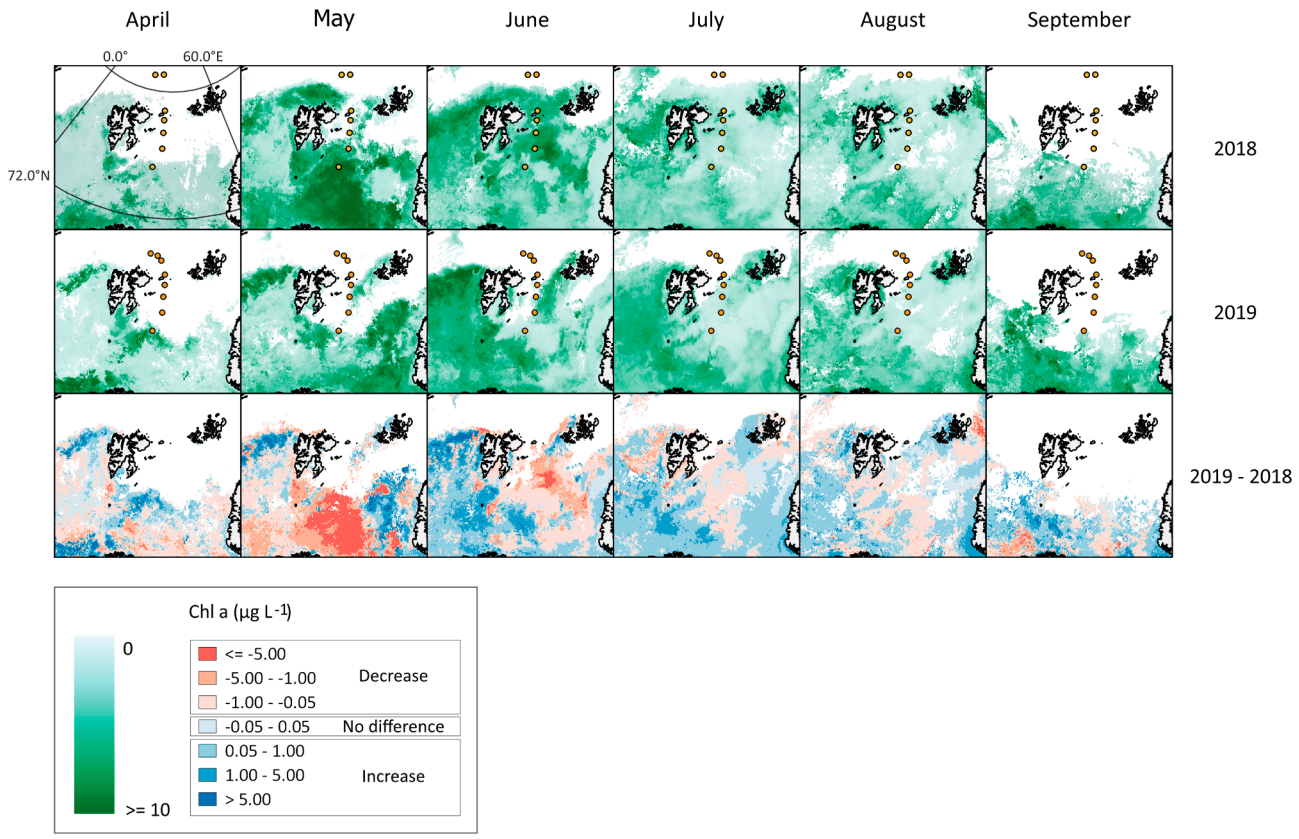

Fig. 3. Satellite-derived monthly composites of surface chl *a* (µg L^{-1}) in the Barents Sea for 2018 (top row), 2019 (middle row) and differences between 2019 and 2018 (bottom row). Sampling stations during both years are represented by the red dots.

Table 2
Loss rate (% d^{-1}) and flux (mg C m^{-2} d^{-1}) at 90 m for the different protist groups along the sampling transects in the northwestern Barents Sea in August 2018 and August 2019 (note: the loss rate calculation at P4 in 2019 is based on integration from 0 to 30 m). 0 = below detection limit.

Parameter	Group	2018				2019				
		P1	P2	P4	PICE1	P1	P4	P5	P6	P7
Loss rate (% d^{-1})	Diatoms	0.2	0	0	2.2	0.6	3.2	65.3	1.2	0.5
	Dinoflagellates	1.2	0.3	4.7	0.8	2.8	2.7	9.5	2.2	0.3
	Other flagellates	4.8	2.2	29.8	1.8	0.9	5.9	10.5	2.0	3.4
	Ciliates	0.2	2.2	0	0	0.3	30.6	0.6	0.1	4.3
Flux (mg C m^{-2} d^{-1})	Diatoms	0.8	0	0	10.1	1.7	3.3	186.5	16.4	3.2
	Dinoflagellates	37.1	6.2	9.2	6.2	20	20.6	68.4	31.1	1.9
	Other flagellates	20.4	7.4	4.1	12.6	10.2	21	44.9	22.1	20.6
	Ciliates	4.3	18.5	0	0	5.0	104.7	1.0	0.2	20.3

2.4. Chlorophyll (chl) a concentrations

Water subsamples for chl *a* concentration measurements were collected at discrete depths (Table 1) from casts taken by a CTD rosette. Water was collected into plastic bottles and stored in a dark and cold location until further processing (within 1 h). Between 0.15 and 1 L of water was filtered through 25 mm Whatman GF/F filters under low vacuum pressure (~30 kPa). Filters were stored in polypropylene tubes with 5 mL of methanol added for chl *a* extraction (overnight at 0–4 °C). Chlorophyll *a* concentrations were measured in the dark according to Holm-Hansen and Riemann (1978) procedure with a Turner Design AU10 fluorometer. The entire chl *a* datasets can be found in Vader (2022).

In order to extend the spatial and temporal coverage of our study, chl *a* surface concentrations (as a proxy for algal biomass) were also estimated by using satellite imagery provided by MODIS-Aqua (Moderate-resolution Imaging Spectroradiometer; 4.6 km resolution data). We used L3 monthly averaged data for the area of interest (71°−80° N, 16°−52° E) for the period of April to September in 2018 and 2019. Near-surface chl *a* concentrations were estimated by using bio-optical models for certain chl *a* ranges. For very clear oligotrophic waters, when chl *a* concentration was below 0.15 mg m^{-3}, the CI (Colour Index) algorithm was applied (Hu et al., 2012), for concentrations above 0.2 mg m^{-3}, the OC3 band ratio model was used (O'Reilly et al., 2000) and between 0.15 and 0.2 mg m^{-3}, a combination of the aforementioned methods was applied. The data can be assessed and downloaded from the NASA (National Aeronautics and Space Administration) OBPG (Ocean Biology Processing Group) archive data website (https://oceancolor.gsfc.nasa.gov/l3/order/). It should be noted that the satellite-derived chl *a* estimates are only valid for the upper surface (~10 m) of the ocean, and are unable to capture the presence of subsurface/deep chl *a* maxima.

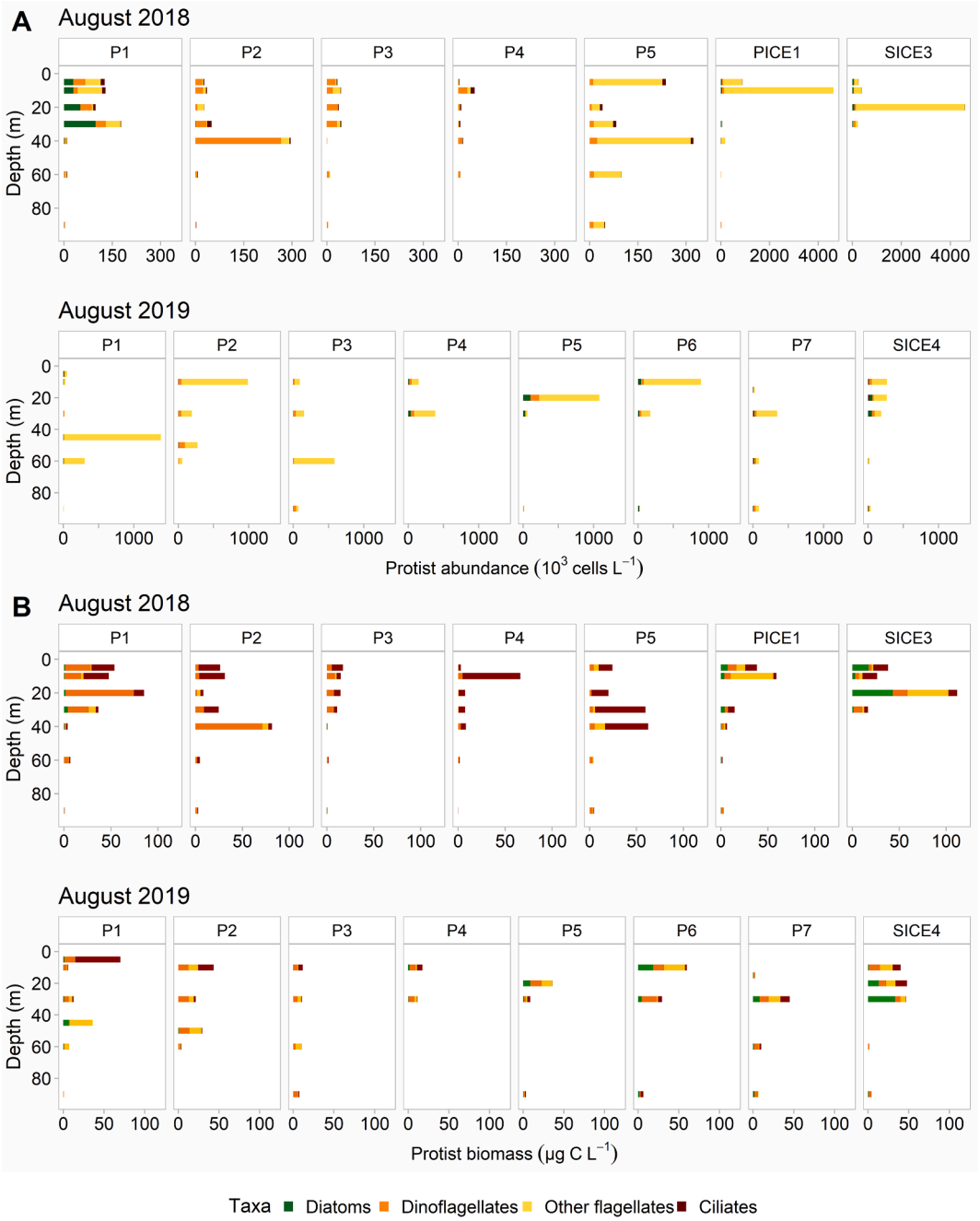

Fig. 4. A) Protist abundances (10^3 cells L^{-1}) and B) biomass (µg C L^{-1}) along the sampling transects in the northwestern Barents Sea in August 2018 (top panels) and August 2019 (bottom panels). Note the difference on the x-axis for the stations PICE1 and SICE3 in 2018.

2.5. *Microbial community composition*

2.5.1. *Light microscopy: Nano- and microplankton communities*

Seawater was collected at discrete depths (Table 1) with Niskin bottles attached to a CTD rosette. For microscopic analysis, 190 mL of seawater from each depth was filled into 200 mL brown glass bottles directly from the Niskin bottles. Samples were fixed with 0.8 mL of 25 % glutaraldehyde and 10 mL of 20 % hexamethylenetetramine-buffered formalin solutions to yield final concentrations of 0.1 and 1 %, respectively. Samples were stored cool (ca. 15 °C) and dark until further processing.

Identification and quantification (cells L^{-1}) of protists were carried out with a Nikon inverted light microscope equipped with phase and differential interference contrasts and objectives 10–60× (resulting in 100–600 × magnification) following the Utermöhl method (Utermöhl, 1958; Edler et al., 2010). Different volumes of sedimentation columns were used (50 mL or 55 mL in 2018; 10 mL, 50 mL or 55 mL in 2019) according to the algal abundance in the samples. Abundances were converted to carbon biomass based on published geometric relationships for biovolume conversion (Hillebrand et al., 1999) and biovolume to carbon conversion factors (Menden-Deuer and Lessard, 2000). Protist community compositions are reported as abundances (cells L^{-1}) and biomass (µg C L^{-1}), and both numerically integrated with a trapezoidal formula over the uppermost 90 m of the water column (standing stocks as cells m^{-2} and g C m^{-2}; note that station SICE3 [0–30 m] in 2018 and stations P2 [0–60 m] and P4 [0–30 m] in 2019 were integrated over shallower depths due to the absence of samples from greater depths). Organisms were identified to the lowest possible taxonomic level and

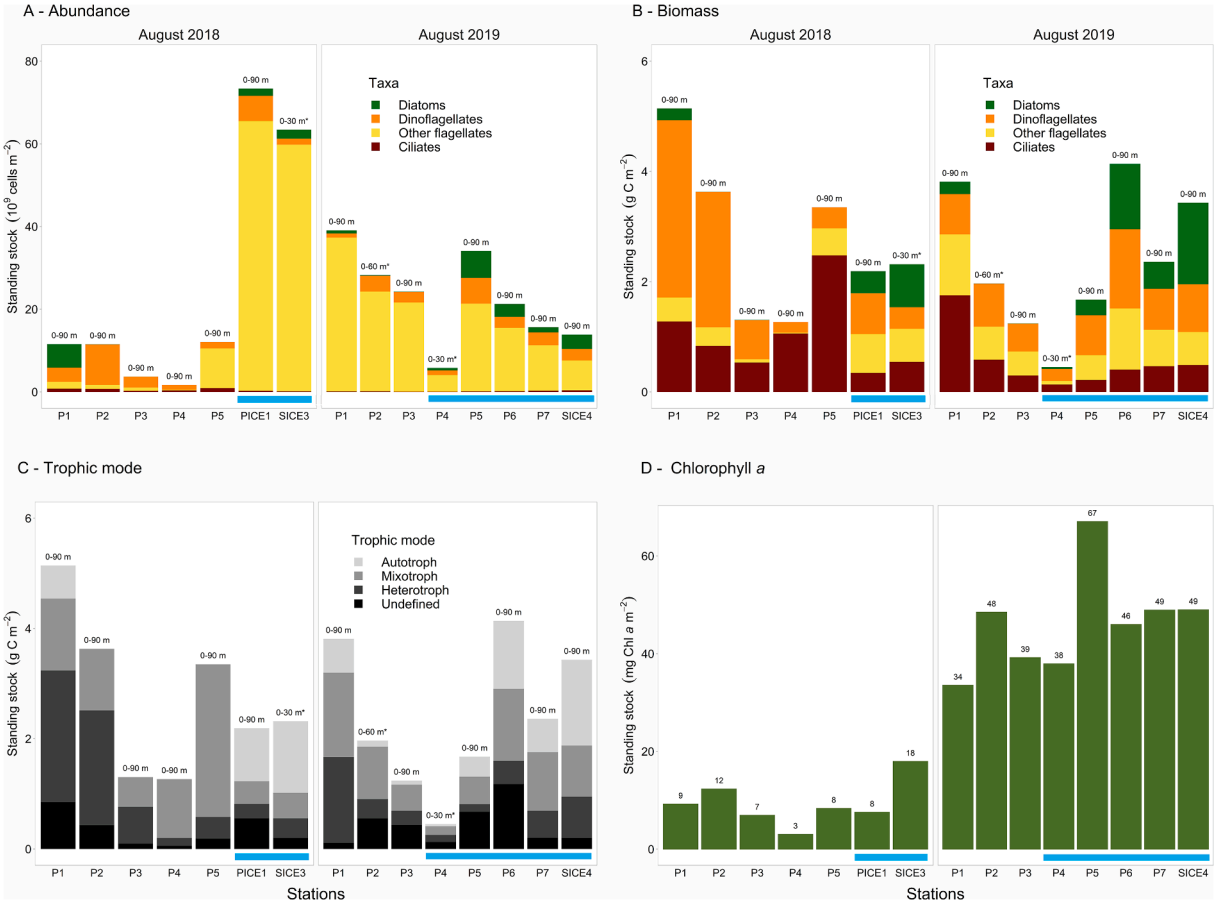

Fig. 5. Depth-integrated stocks of A) protist abundances (10^9 cells m^{-2}), B) biomass (g C m^{-2}), C) trophic mode (g C m^{-2}) and D) chl *a* (mg m^{-2}) for the upper 90 m surface layer along the sampling transects in the northwestern Barents Sea in August 2018 (left panels) and August 2019 (right panels). *For stations SICE3 in 2018, and P2 and P4 in 2019, protist stocks were integrated over shallower depth. Blue lines indicate stations that were sea ice-covered during the time of sampling.

were named according to the World Register of Marine Species (WoRMS). Protist taxonomy data can be found in Assmy et al. (2022a) for JC1_2 and Assmy et al. (2022b) for Q3.

2.5.2. *Flow cytometry: Pico- and nanophytoplankton communities*

Seawater was collected at discrete depths (Table 1) with Niskin bottles attached to a CTD rosette. Samples for flow cytometric abundance analysis were prepared in triplicates by fixing 1.8 mL of seawater with 36 µL 25 % glutaraldehyde (0.5 % final concentration) at 4 °C in the dark for a minimum of 2 h, then flash-frozen in liquid nitrogen and stored at −80 °C until further processing.

The abundances of pico- and nano-sized phytoplankton and heterotrophic nanoflagellates (HNF) were determined using an Attune® NxT, Acoustic Focusing Cytometer (Invitrogen by Thermo Fisher Scientific) with a syringe-based fluidic system and a 20 mW 488 nm (blue) laser. Pico- and nanophytoplankton were counted after thawing the sample and the various groups of protists were discriminated based on their red fluorescence (BL3) *vs.* orange fluorescence (BL2), red fluorescence (BL3) *vs.* side scatter (SSC) and orange fluorescence (BL3) *vs.* side scatter (SSC) (Paulsen et al., 2016). For HNF analysis, samples were stained with SYBR Green I for 2 h in the dark and subsequently 1–2 mL was measured at a flow rate of 500 µL min^{-1} following the protocol of Zubkov et al. (2007). Pico- and nanophytoplankton community compositions are reported as cells mL^{-1} and abundance was converted into biomass (µg C L^{-1}). HNF biomass was estimated using 0.220 pg C $µm^{-3}$ as conversion factor (Børsheim and Bratbak,1987). Biomass of pico- and nanophytoplankton was calculated using equivalent spherical diameter (ESD) to estimate cell volume (CV) and the formula Carbon per cell [pg C $cell^{-1}$] = 0.216 × $CV^{0.939}$ to calculate carbon content (Mullin et al., 1966; HELMCOM-Guidelines for monitoring of phytoplankton species composition, abundance, and biomass 2021). ESDs for the three phytoplankton size groups were estimated using a bead mix (1, 2, 4, 6 and 15 µm) during flow cytometry and are given as average based on the estimated upper and lower limits of the gates of the different phytoplankton groups (picophytoplankton [size range 0.2–2 µm]: r = 0.55 µm; small nanophytoplankton [2–5 µm]: r = 1.75 µm; larger nanophytoplankton [5–10 µm]: r = 3.75 µm).

2.5.3. *Vertical flux*

Short-term sediment traps (KC-Denmark, 2–4 cylinders, aspect ratio > 6) were deployed at six different depths at stations P1, P2, P4 and PICE1 in August 2018 and at stations P1, P4, P5, P6 and P7 in August 2019 (Table 1). Before the deployment, the cylinders were filled with high-salinity deep water that was collected at the station and filtered through GF/F filters in order to minimize flushing during deployment and recovery. The sediment traps were freely drifting in open water or anchored to an ice floe in ice-covered waters to facilitate a semi-Lagrangian drift. Deployment times varied from 19 to 41 h, with shorter deployment periods in order to minimize particle degradation when a high amount of sinking material was expected, and longer periods when little material was expected to sink out. No preservatives were used during deployment. After retrieval, contents of cylinders from the same depth were pooled in one carboy. The samples were stored at 4 °C until further processing within 20 h after the retrieval. After homogenizing, a 100 mL water sample was fixed with a glutaraldehyde-lugol solution (Rousseau et al., 1990) and stored at 4 °C in the dark. Protist communities were analysed microscopically as described in section 2.5.1 and daily flux rates are reported as cells m^2 d^{-1} and

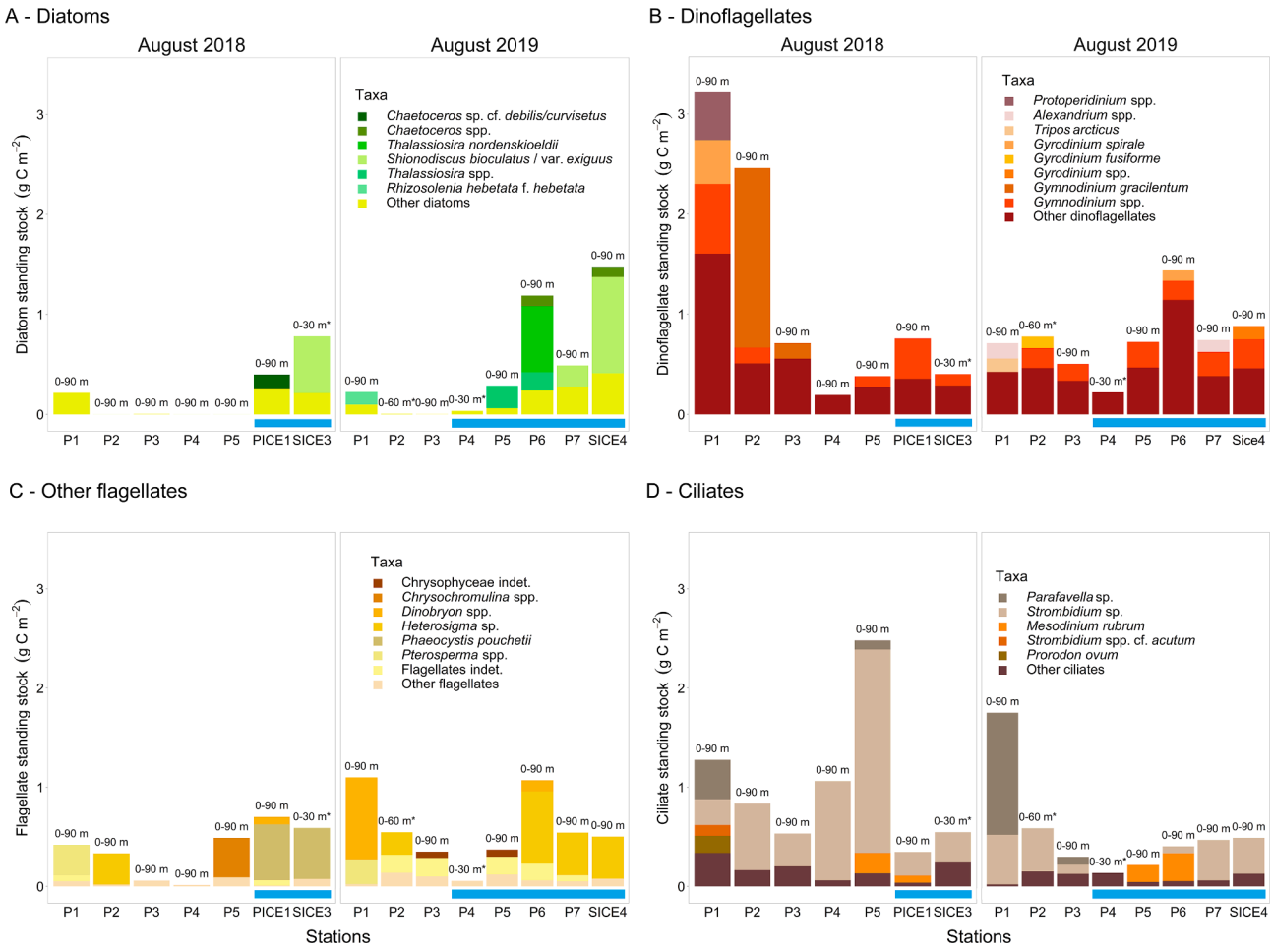

Fig. 6. Depth-integrated stocks of protist biomass (g C m^{-2}) for the upper 90 m surface layer representing A) diatoms, B) dinoflagellates, C) other flagellates, and D) ciliates along the sampling transects in the northwestern Barents Sea in 2018 (left) and 2019 (right). * For stations SICE3 in 2018, and P2, P4 in 2019, protist stocks were integrated over shallower depth. Blue lines indicate stations that were sea ice-covered during the time of sampling.

biomass as mg C m^{-2} d^{-1}.

The relative daily loss rates at 90 m depth were calculated as:

$$\%\ Loss\ rate\ d^{-1} = \left(\frac{flux\ at\ 90m\ [mg\ C\ m^{-2}\ d^{-1}]}{integrated\ standing\ stock\ (0-90m)\ [mg\ C\ m^{-2}]}\right)*100$$

3. Results

3.1. Sea-ice conditions

The ice conditions in August 2018 and August 2019 differed substantially (Fig. 1, Table A.1). During the sampling in 2018, sea ice occurred mainly in the Arctic Basin, north of the shelf break, while in 2019, also large parts of the northwestern Barents Sea shelf were ice-covered.

According to sea ice observations from the bridge, areas represented by sampling stations P1 to P5 were ice-free in 2018. The ice edge (10 % ice cover) was encountered at ca. 82.9°N and 31.4°E. All the remaining stations were covered by ice from 70 to 100 %. First-year ice (FYI) with a thickness of around 1.0 m dominated at station PICE1, while second-year ice with a thickness of 1.7–1.8 m dominated at station SICE3. Sea ice was covered by a thin, around 2 cm thick snow cover, and melt ponds covered 10–30 % of the surface of the ice floes. At the ice-covered stations, open water areas were limited to leads of 50 to 200 m width.

In 2019, ice extended much further south and only stations P1 to P3 were ice free. The ice edge was encountered between two ice observations: 79.1°N and 34.0°E (0 % ice cover) and 79.8°N and 34°E (60 % ice cover). Ice concentration, dominated by FYI < 0.7 m thickness and narrow leads of open water <200 m wide, increased from 60 % to 90 % between P4 and P6. While areas at P7 had similar conditions to those represented by station P6, less ice (70 % cover) occurred further west, where sampling station SICE4 was located, with open water in narrow leads of 50–200 m width. FYI < 0.7 m dominated in the entire area (for more details see Van Engeland et al., submitted for publication, same issue).

3.2. Temperature, salinity, and inorganic nutrients

In 2018 and 2019, Atlantic water dominated the water column south of the Polar Front (station P1) while surface waters further north were fresher polar water masses (Fig. 2A, B). Temperature-salinity distribution at stations P2-P5 indicated that the relatively warm upper ocean north of the Polar Front was a result of surface warming rather than intrusion of Atlantic Water (Fig. A.1). Coldest and least saline surface water was observed at the northernmost stations, most evident in 2019. Shoaling of warm Atlantic water was observed at the shelf break (station P6) and in the southern Nansen Basin (station P7) indicative of the Svalbard branch of Atlantic water entering the Arctic Ocean along the shelf break north of Svalbard. The nutricline of nitrate, silicate and phosphate was generally deeper in 2018 (50 m) compared to 2019 (20–30 m), except at the permanently open water station P1 and station P2 just north of the polar front (Fig. 2C-E). In 2018, surface nutrient concentrations were still elevated (nitrate > 4 μM) at the two

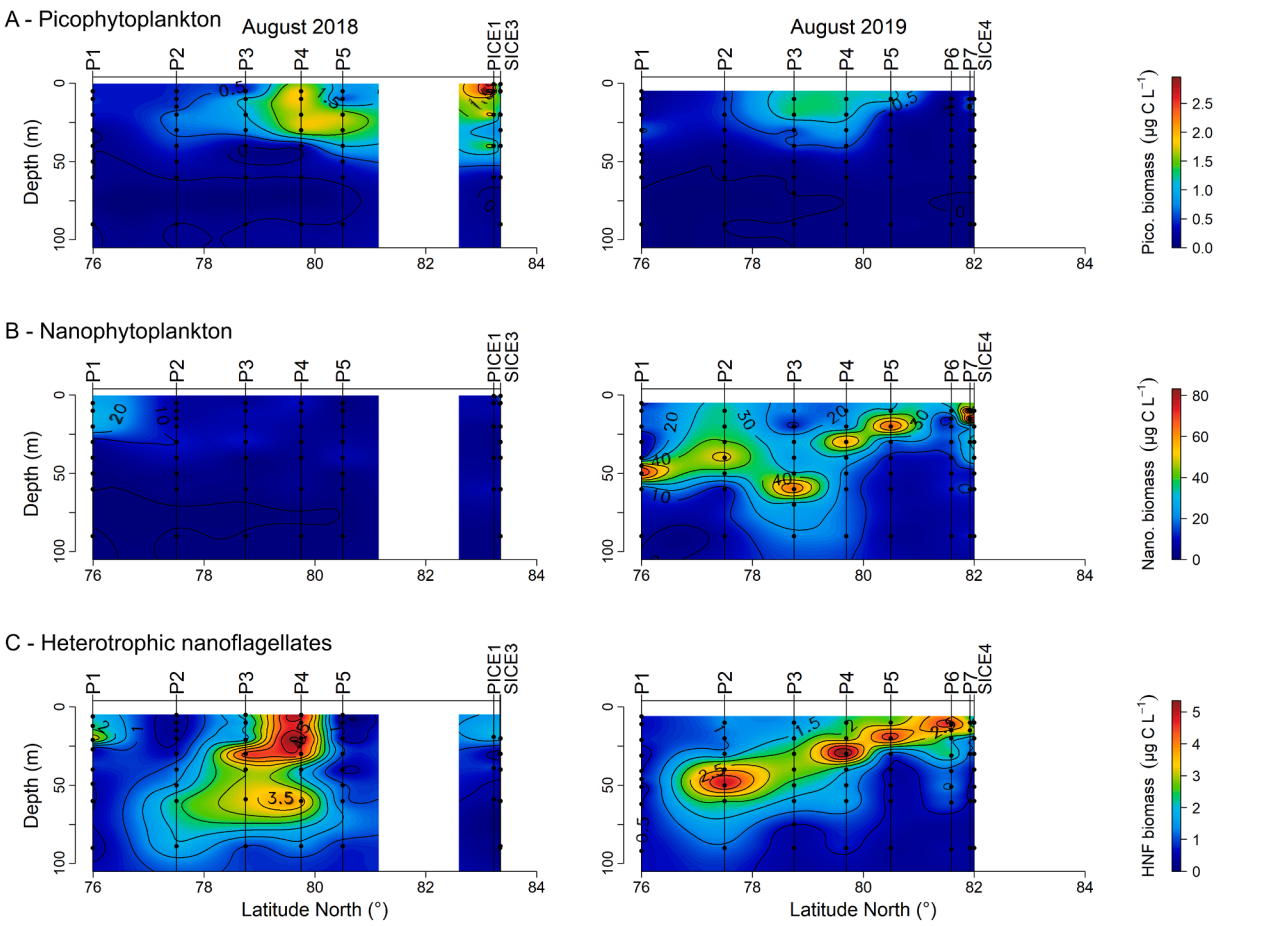

Fig. 7. Cell biomass of small phytoplankton and heterotrophic nanoflagellates (0.2 – 10 µm) along the sampling transects in the northwestern Barents Sea in 2018 (left panels) and 2019 (right panels) divided according to trophy and size into A) picophytoplankton (0.2–2 µm), B) nanophytoplankton (2–10 µm) and C) heterotrophic nanoflagellates.

northernmost ice stations. However, it needs to be noted that those stations were about 1° latitude further north than the sea ice stations P6 and P7 in 2019 due to the northward retreat of the ice edge in August 2018 and hence not directly comparable.

3.3. Chlorophyll *a* concentrations

Chlorophyll *a* concentrations and standing stocks were overall lower in 2018 compared to 2019, reaching maximum values in the upper 10 m at station PICE1 in 2018 (0.87 to 1.09 µg L^{-1}) and peaked at station P5 with 2.57 µg L^{-1} at 20 m in 2019 (Fig. 2F). In both years, the values were the highest in the top 60 m of the water column. In 2019, chl *a* concentrations at the ice-covered stations reached their maximum in surface waters (Fig. 2F).

Monthly chl *a* climatologies were derived from remote sensing data for 2018 (top row), 2019 (middle row) as well as differences between 2019 and 2018 (bottom row; Fig. 3). The grey and white colours correspond to the land and cloud masks, respectively. An extensive phytoplankton bloom was observed in May 2018. Aggregation and decaying phytoplankton in large bloom events will result in increased backscatter, which impacts the chl *a* retrieval models used here. Hence, the actual chl *a* values might have been lower, but our data suggest a significant bloom in May. The difference map (bottom row) for May shows markedly lower chl *a* concentrations in 2019 compared to 2018 (dark blue colour). In the area of interest (71°– 80° N, 16°–52° E), in May 2018, the average chl *a* value was 5.2 ± 6.5 mg m^{-3}, while in May 2019 the average chl *a* value was 1.7 ± 2.1 mg m^{-3}. This shows that on average the difference in chl *a* content corresponds to 3.5 mg m^{-3} (Table A.2). Besides this event in May 2018, a general increase in certain areas can be observed (red colour in Fig. 3, bottom row) or no difference (green colour in Fig. 3, bottom row) in the chl *a* content over the entire seasonal production cycle (Table 2).

3.4. Protist community composition

All identified protist taxa from Niskin bottle samples are presented in Table A.3.

Protist abundances were overall higher in August 2019 compared to August 2018, except at the ice-covered stations PICE1 and SICE3, where abundances in 2018 exceeded those in 2019 and were about one order of magnitude higher compared to values observed at open-water areas in 2018 (Fig. 4A). In contrast, the overall biomass was higher in 2018 compared to 2019 (Fig. 4B). In both years, (depth-integrated) algal abundances and biomass were the lowest at stations P3 and P4 (note: in 2019, data only available from 0 to 30 m; Figs. 4B, 5A, B). In 2018, heterotrophic taxa clearly dominated the protist community, except for the two ice-covered stations where autotrophic taxa prevailed (Fig. A.2), while in 2019, the majority of the community was auto- or mixotrophic (Fig. 5C, A.**2**).

In 2018, diatoms numerically predominated the protist community at the southernmost station (P1), dinoflagellates dominated further north (stations P2 to P4), whereas other flagellates (primarily prymnesiophytes) dominated at the northernmost stations (P5 to SICE3). In turn, in 2019, flagellates dominated numerically the entire study area (Fig. 4A, 5A). Chrysophyte flagellates were highly abundant at station P5 in 2018 and P1 in 2019 but contributed less to the biomass at these

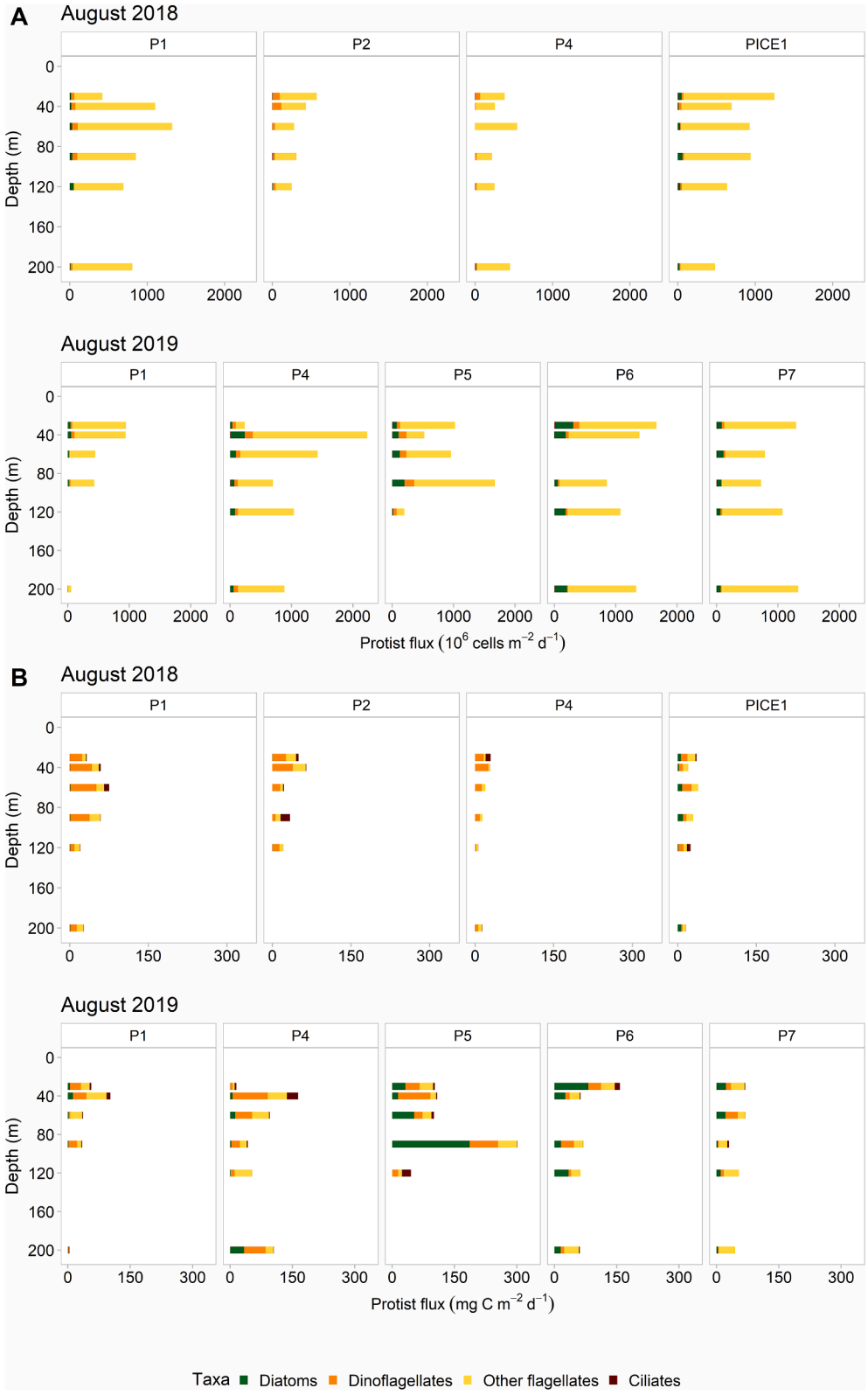

Fig. 8. Vertical flux of protist A) abundances (10^6 cells m^{-2} d^{-1}) and B) biomass (mg C m^{-2} d^{-1}) at selected depths for the upper 200 m of the water column along the sampling transects in the northwestern Barents Sea in August 2018 (top panels) and August 2019 (bottom panels). Note: data not available for all stations.

stations (Fig. A.3). In terms of biomass, dinoflagellates and ciliates dominated in the ice-free areas (stations P1 to P5) and other flagellates dominated at the two ice-covered stations in 2018 (PICE1 and SICE3; Fig. 4B, 5B). In 2019, dinoflagellates and oligotrich ciliates dominated protist biomass in open-waters at stations P1 to P3 and in the proximity of the ice edge (station P4), while diatoms were a prominent component of the protistan community in the ice-covered areas (stations P5 to P7; Fig. 4B, 5B). Diatom biomass was the highest in the uppermost 40 m at the ice-covered stations during the two years of observations.

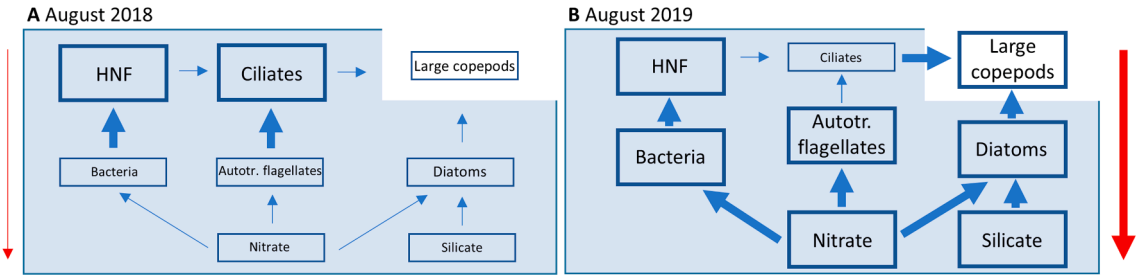

Fig. 9. Biomass distribution in the microbial food web (Conceptual model after Thingstad et al., 2020) and vertical particle flux in the northwestern Barents Sea in **A)** August 2018 and **B)** August 2019 considering stations P2 to P5 representative of the interior shelf (north of the polar front and south of the continental slope). Box sizes indicate differences in biomass (for bacteria, protists, copepods) and nutrient concentrations (small = low, large = high). Mixotrophic nanoflagellates are included under autotrophic flagellates. Blue arrows indicate flow between the different components of the microbial food web where the thickness of the arrows indicates the strength of the flow from food to consumer. Vertical flux of protists is represented by red arrows (thicker arrow indicates higher protist flux). Future longer open water oligotrophic seasons (as seen in 2018) are likely to strengthen the left-hand side of the food web model comprising smaller forms relative to the more energy-efficient pathway of larger diatoms to the *Calanus* food web (as seen in 2019). Lower biomass and dominance of small-celled protists result in lower vertical flux. Our data indicate a strong trophic relationship between mixotrophic ciliates (*Strombidium*, *Mesodinium*) and autotrophic flagellates in both years. HNF were main grazers of bacteria.

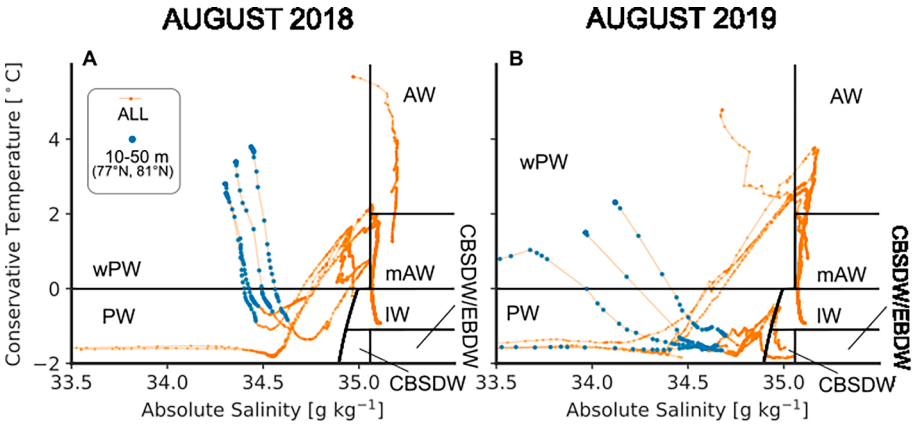

Fig. A1. Distribution of Conservative Temperature and Absolute Salinity below 10 m depth from CTD profiles collected at the station locations in the northwestern Barents Sea (Fig. 1) during the two cruises. Water mass categories from Sundfjord et al. (2020) are shown as black boxes. Blue circles highlight measurements from < 50 m depth and between 77°N and 81°N (stations P2-P5). Due to intermittent sensor issues, the profile from station P7 in 2019 was replaced by a profile taken 7.5 km to the northeast.

3.4.1. Diatoms

Diatoms contributed to overall biomass to a larger extent in 2019 than in 2018 (Fig. 4B). In both years, the highest diatom standing stocks were observed at the ice-covered stations (Fig. 5B). It is noteworthy that diatom standing stocks were similar in both years at the ice-free station P1, dominated by Atlantic water masses, and at the same time considerably higher than at the open-water stations (P2 and P3) north of the Polar Front (Fig. 5B).

In 2018, the diatom community was primarily represented by *Leptocylindrus minimus* in Atlantic waters (station P1), followed by *Pseudo-nitzschia* spp., which dominated also in ice-covered waters (station SICE3). Interestingly, both taxa did not contribute largely to the diatom community in 2019 (Fig. 6A, Fig. A.4A). In comparison to 2018, species of the genus *Fragilariopsis* were abundant in 2019, particularly at the ice-covered stations P4 and P5. Important contributors to phytoplankton biomass in 2019 were species of *Thalassiosira*, especially in ice-covered waters represented by stations P4 to SICE4 (Fig. 6A). A species commonly found in both pelagic and sea ice-associated communities, *Shionodiscus biocolatus* (formerly *Thalassiosira bioculata*), contributed largely to the diatom biomass at the northernmost ice-covered stations in both years (SICE3 in 2018 as well as P7 and SICE4 in 2019). The oceanic diatom *Rhizosolenia hebetata* f. *semispina* was a dominant component of the diatom community at the open-water station P1 in 2018 and at the ice-covered stations P5 to P7 in 2019, while *Rhizosolenia hebetata* f. *hebetata* dominated at P1 in 2019 (Fig. 6A). *Chaetoceros* species contributed moderately to the protistan biomass at the ice station PICE1 in 2018 and P6 and SICE4 in 2019.

3.4.2. Dinoflagellates

Highest dinoflagellate standing stocks were found at the southernmost stations on either side of the Polar Front (P1 and P2) in 2018 (Fig. 5B). In other areas, interannual differences were not very pronounced and dinoflagellate standing stocks varied between 0.19 and 3.21 g C m^{-2}. Athecate dinoflagellates (naked or unarmoured) dominated dinoflagellate biomass in both years, except for station P1 in 2019. Thecates were also important at station P5 in 2019 (Fig. A.5). Among the athecate dinoflagellates, gymnodinoid species were high in numbers and biomass in both years (Fig. 6B, Fig. A.4B). Another numerically important component were thecate dinoflagellates of the genus *Heterocapsa*, which were more abundant in 2019 than in 2018, particularly at station P2 (Fig. A.4B). Peridiniales had an overall higher biomass in 2019 *vs.* 2018.

3.4.3. Other flagellates

Dominance in the phylogenetically diverse flagellate community was quite variable across the transect in both years (Fig. 6C, Fig. A.4C). In 2018, the flagellate community at the ice stations PICE1 and SICE3 was dominated by the prymnesiophyte *Phaeocystis pouchetii*, both in numbers and biomass, which was distinctly less abundant in 2019 (Fig. 6C, Fig. A.4C). The raphidophyte *Heterosigma* sp. dominated the flagellate biomass at the ice-covered stations P6 to SICE4 in 2019 and at station P2 in 2018. At station P5, the prymnesiophyte *Chrysochromulina* sp. dominated in 2018. At station P1, the prasinophyte *Pterosperma* sp. dominated in 2018 while the chrysophyte *Dinobryon* sp. was a dominant component in 2019 (Fig. 6C).

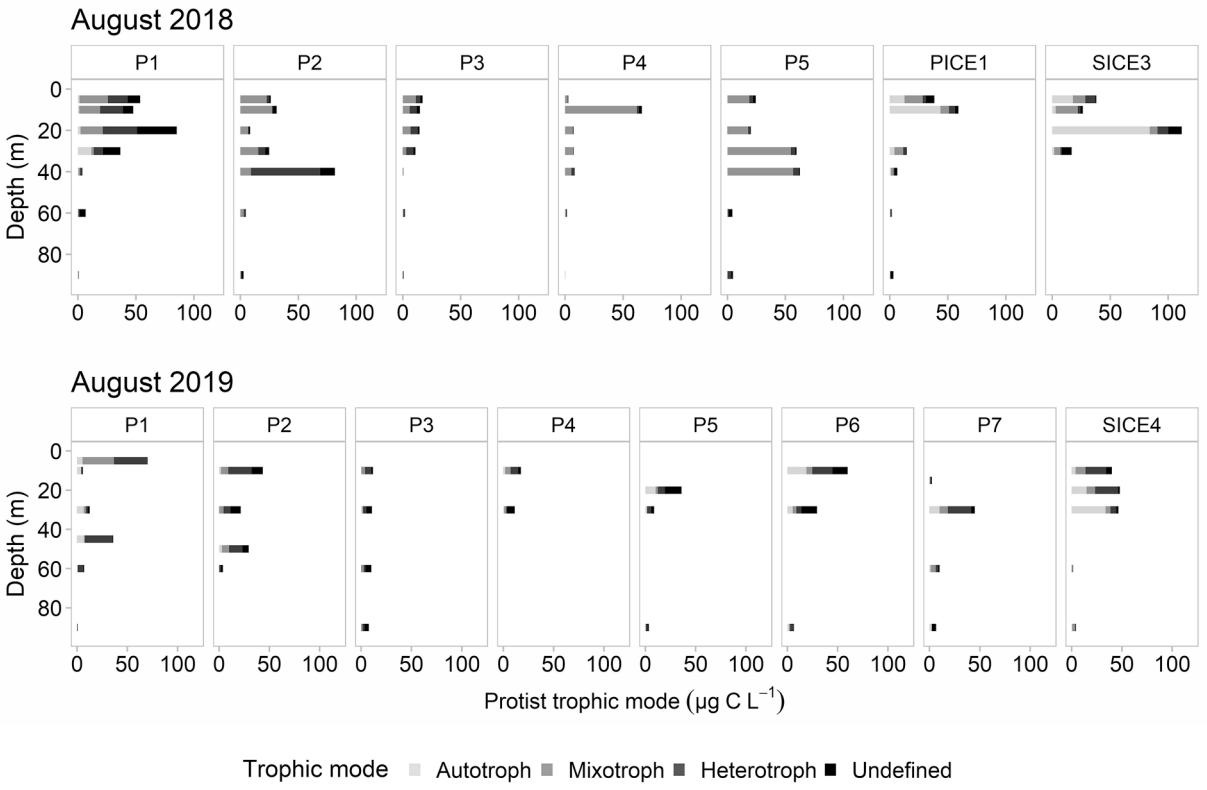

Fig. A2. Protist trophic mode (µg C L^{-1}) per depth (m) along the sampling transects in the northwestern Barents Sea in August 2018 (top panels) and August 2019 (bottom panels).

3.4.4. *Ciliates*

Ciliate biomass was generally higher in 2018 than in 2019, except at the southernmost station P1 and the northernmost ice-covered areas, where ciliate standing stocks were similar in both years (Fig. 5B, 6D). The genus *Strombidium* dominated the ciliate biomass at most stations in both years (Fig. 6D), and also in numbers at stations P2, P4 and P5 in 2018, as well as SICE4 in 2019 (Fig. A.4D). *Parafavella* sp. contributed largely to the ciliate biomass at station P1, particularly in 2019. Mixotrophic *Mesodinium rubrum* dominated ciliate standing stocks at stations P5 and P6 in 2019.

3.5. *Pico- and nanophytoplankton community composition*

Abundances of autotrophic organisms in the size range of 0.2 – 10 µm were determined using flow cytometry, with highest abundances measured at depths corresponding to the chl *a* maximum and above. Data were grouped into pico- and small nano-sized phytoplankton (0.2–2 µm and 2–10 µm, respectively) and visualized as cell biomass (µg C L^{-1}) for the upper 100 m of the transects in 2018 and 2019 in Fig. 7. Dominating size groups were different during the contrasting years and picophytoplankton biomass was the highest in 2018, with up to 2.5 µg C L^{-1} at the ice-covered station SICE3 (Fig. 7A). Picophytoplankton abundances in 2018 increased gradually from south to north, with 2000 cells mL^{-1} at station P1, 4000 cells mL^{-1} at station P2, 7000 cells mL^{-1} at station P3 until 12,000 cells mL^{-1} at station P4 and decreasing thereafter before highest abundances were detected at station SICE3 (19,000 cells mL^{-1}; Fig. A.6). Picophytoplankton abundances measured in 2019 were comparable in terms of spatial pattern, but overall values were lower than in 2018.

Nanophytoplankton was generally more abundant in 2019 than 2018, with biomass concentrations of up to 80 µg C L^{-1} at station P7 in 2019 (Fig. 7B). Highest biomass in 2018 was measured furthest south (station P1) with around 30 µg C L^{-1}. In 2019, the nanoplankton biomass pattern corresponded to the chl *a* maximum.

Biomass of heterotrophic nanoflagellates (HNF) was comparable in 2018 and 2019 with peaks at around 4–5 µg C L^{-1} (Fig. 7C). In 2018, highest concentrations were at stations P3 and P4, while in 2019, highest biomass coincided with the chl *a* maximum, peaking at stations P2, P4, P5 and P6.

3.6. *Vertical flux of protist communities*

All identified protist taxa from sediment trap samples are presented in Table A.4.

Both protist cell and biomass vertical flux were higher in 2019 than in 2018 (Fig. 8). The vertical flux of cells ranged from 195 to 2184 10^6 cells m^{-2} d^{-1} in 2019 and from 215.7 to 1306 10^6 cells m^{-2} d^{-1} in 2018 across all depths. The only exception was P1 in 2019, where cell fluxes were lower than in 2018, and a strong flux attenuation from 932 10^6 cells m^{-2} d^{-1} at 30 m to 54.1 10^6 cells m^{-2} d^{-1} at 200 m depth. The vertical flux of protist biomass ranged from 4.6 to 198 mg C m^{-2} d^{-1}, except for one station in 2019 with high flux dominated by diatoms (station P5 at 90 m with 296 mg C m^{-2} d^{-1}; Fig. 8B).

In general, flagellates dominated cell fluxes at all stations in both years (Fig. 8A, Fig. A.7A). This reflected mostly the pattern in the suspended communities; except for stations P1 to P4 in August 2018, where diatoms and/or dinoflagellates dominated the suspended communities, whereas the sinking cells were dominated by flagellates. Despite the dominance of flagellates in terms of cell flux, dinoflagellates contributed more to the carbon flux. Diatom carbon flux was higher in 2019 than in 2018, particularly at stations P5 and P6, both in numbers and biomass (Fig. 8A, B).

Interestingly, the stations with the highest biomass in the suspended communities were not always dominated by diatoms but rather by dinoflagellates and flagellates, although this was not reflected in the protist carbon flux. The highest protist carbon flux was measured in

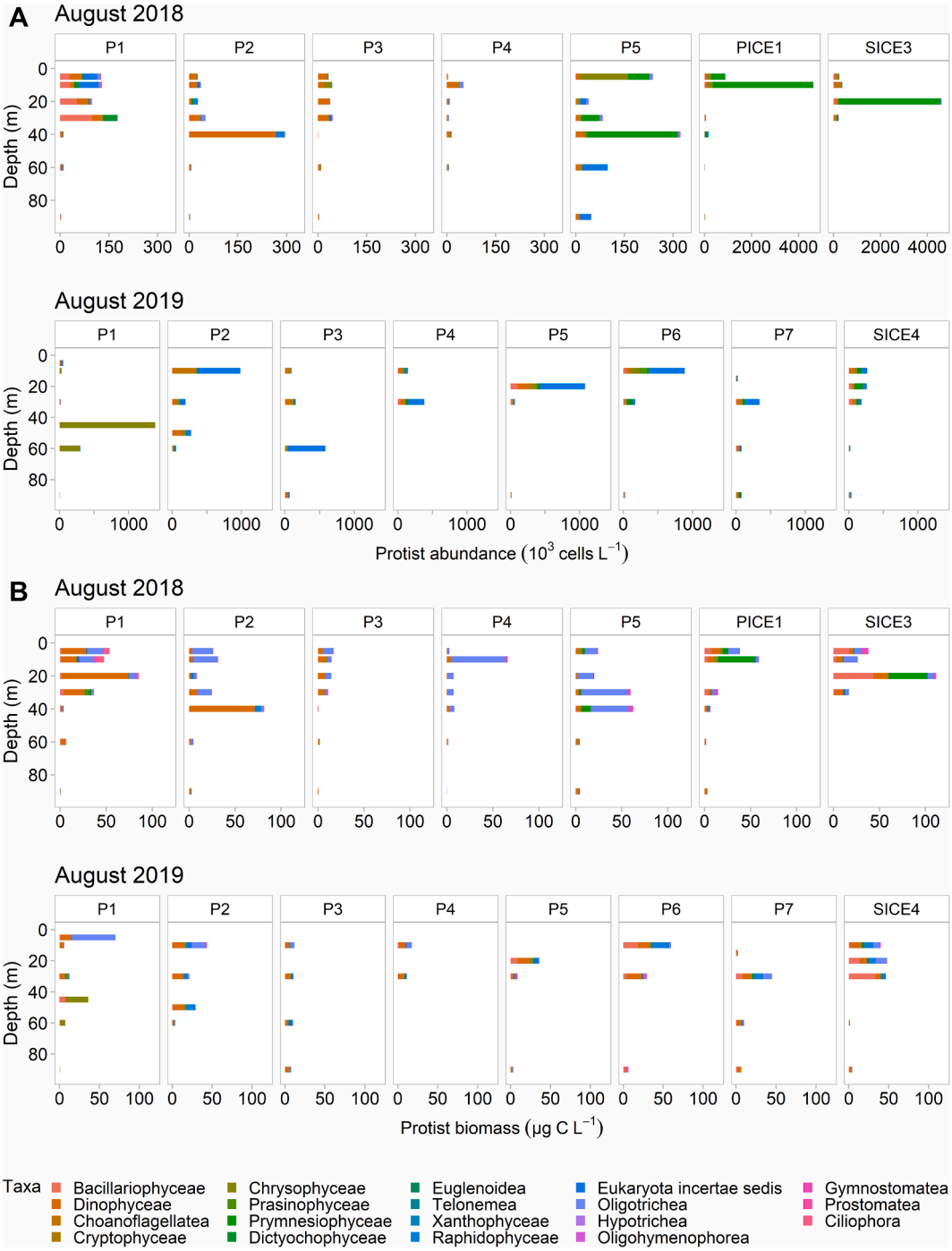

Fig. A3. Protist A) abundances (10^9 cells m^{-2}) and B) biomass µg (C L^{-1}) per depth (m) of all identified taxa along the sampling transects in the northwestern Barents Sea in August 2018 (top panels) and August 2019 (bottom panels). Note the difference on the x-axis for the stations PICE1 and SICE3 in 2018.

August 2019 at station P5 at 90 m and was dominated by diatoms of the genus *Thalassiosira* (Fig. 8B, Fig. A.7B). In 2018, cell flux at the southernmost station P1 and the northernmost ice-covered station PICE1 was dominated by prymnesiophytes (particularly *Phaeocystis pouchetii*; Fig. A.7A), however, in terms of carbon flux, dinoflagellates dominated at P1 and PICE1, represented by a mixed community (Fig. 8B). *Fragilariopsis* spp. and *Chaetoceros* spp. dominated diatom cell flux at stations P1 and PICE1, respectively, but due their relatively small size, diatoms contributed little to carbon flux at those stations.

Loss rates at 90 m were the highest in 2019 at station P4, dominated by ciliates (>30 % relative to suspended communities) and station P5, dominated by diatoms (>60 %), and in 2018 at P4, dominated by flagellates (>30 %, Table 2).

Although average total particulate organic carbon (POC) flux was comparable in both years (Amargant-Arumí et al. in prep., same issue), protist carbon flux in 2018 contributed much less to total POC flux compared to 2019, with a mean of 25.8 % ± 18.9 in 2018 *vs.* a mean of 54.6 % ± 25.1 in 2019 considering all stations and depths.

4. Discussion

4.1. Contrasting late summer environmental conditions

Large interannual variability in sea-ice cover and oceanographic

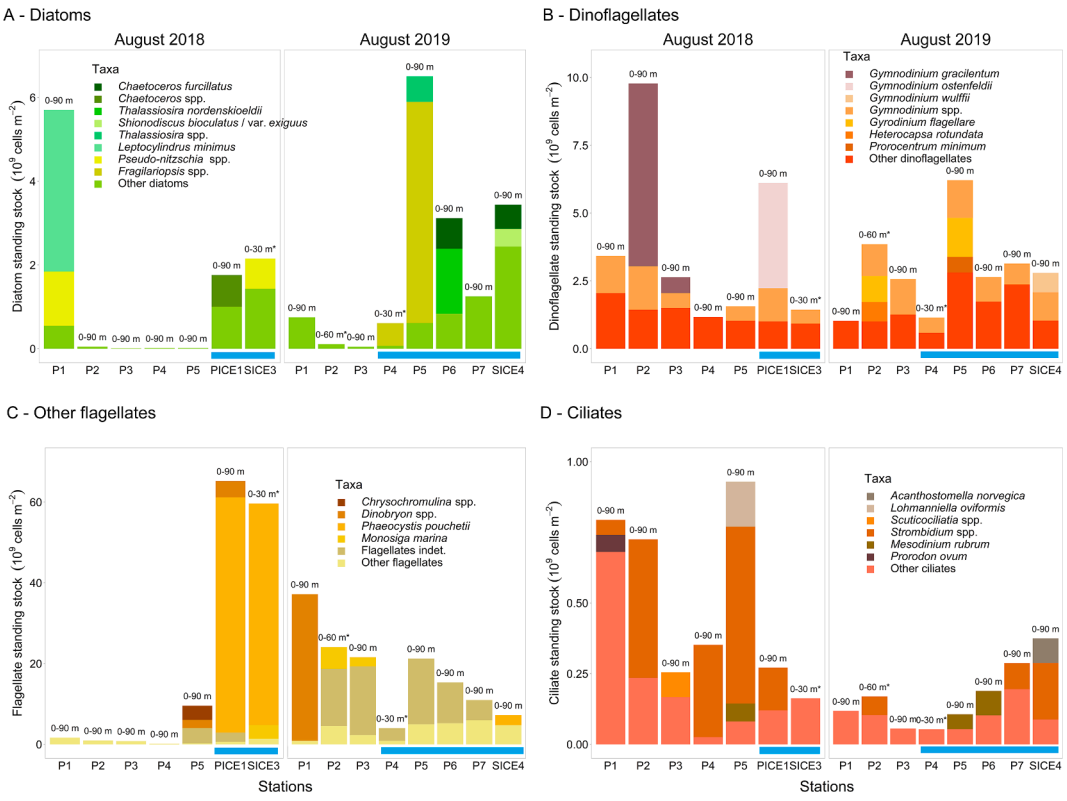

Fig. A4. Depth-integrated stocks of protist abundances (10^9 cells m^{-2}) for the upper 90 m surface layer representing A) diatom species, B) dinoflagellate species, C) other flagellates, and D) ciliate species along the sampling transects in the northwestern Barents Sea in 2018 (left) and 2019 (right) *For stations SICE3 in 2018, and P2 and P4 in 2019 integrated stocks were integrated over shallower depth. Note the difference on the y-axes. Blue lines indicate stations that were sea ice-covered during the time of sampling.

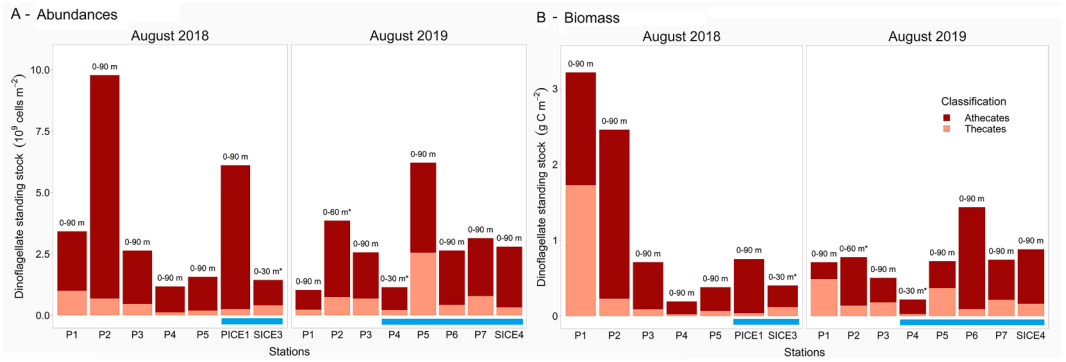

Fig. A5. Depth-integrated stocks of dinoflagellate A) abundances (10^9 cells m^{-2}) and B) biomass μg (C L^{-1}) per depth classified in athecates and thecates along the sampling transects in the northwestern Barents Sea in August 2018 and August 2019. *For stations SICE3 in 2018, and P2 and P4 in 2019 integrated stocks were integrated over shallower depth. Blue lines indicate stations that were sea ice-covered during the time of sampling.

conditions is typical for the Barents Sea (Falk-Petersen et al., 2000; Furevik, 2001; Serykh and Kostianoy, 2019). The two sampling years 2018 and 2019 offer a prime example for these annual fluctuations, characterized by contrasting environmental conditions, including sea-ice cover, sea-water temperature, and salinity as well as nutrient availability.

Despite sampling during the same time of the year, the earlier sea-ice retreat and longer open water summer season in 2018 caused differences in the timing of seasonal succession and thus in the composition of the pelagic protist communities in late summer (Figs. 4-6). This is corroborated by previous studies from other seasonally ice-covered regions of the Arctic Ocean showing a link between seawater temperature, sea-ice cover and protist phenology (Nöthig et al., 2015; Dąbrowska et al., 2020). In the Barents Sea, the spring bloom typically occurs in May, starting in the permanently ice-free areas with elevated concentrations along the ice-edge rather than in ice-free areas (Engelsen et al., 2002), indicating that meltwater-induced stabilization of the water column has a positive effect on primary production (Qu et al., 2006). The earlier onset and more intense spring bloom in 2018 as evidenced from satellite-derived chl *a* (Fig. 3) can be attributed to the earlier ice retreat compared with 2019. Hence, the protist community in August 2018 was in a seasonally later stage of its succession than in August 2019. The interannual differences in chl *a* revealed by our *in situ* observations are not reflected in the satellite data which show similar chl *a* values in August for both years. However, it needs to be considered that satellites do not capture the subsurface chl *a* maximum that largely accounted for

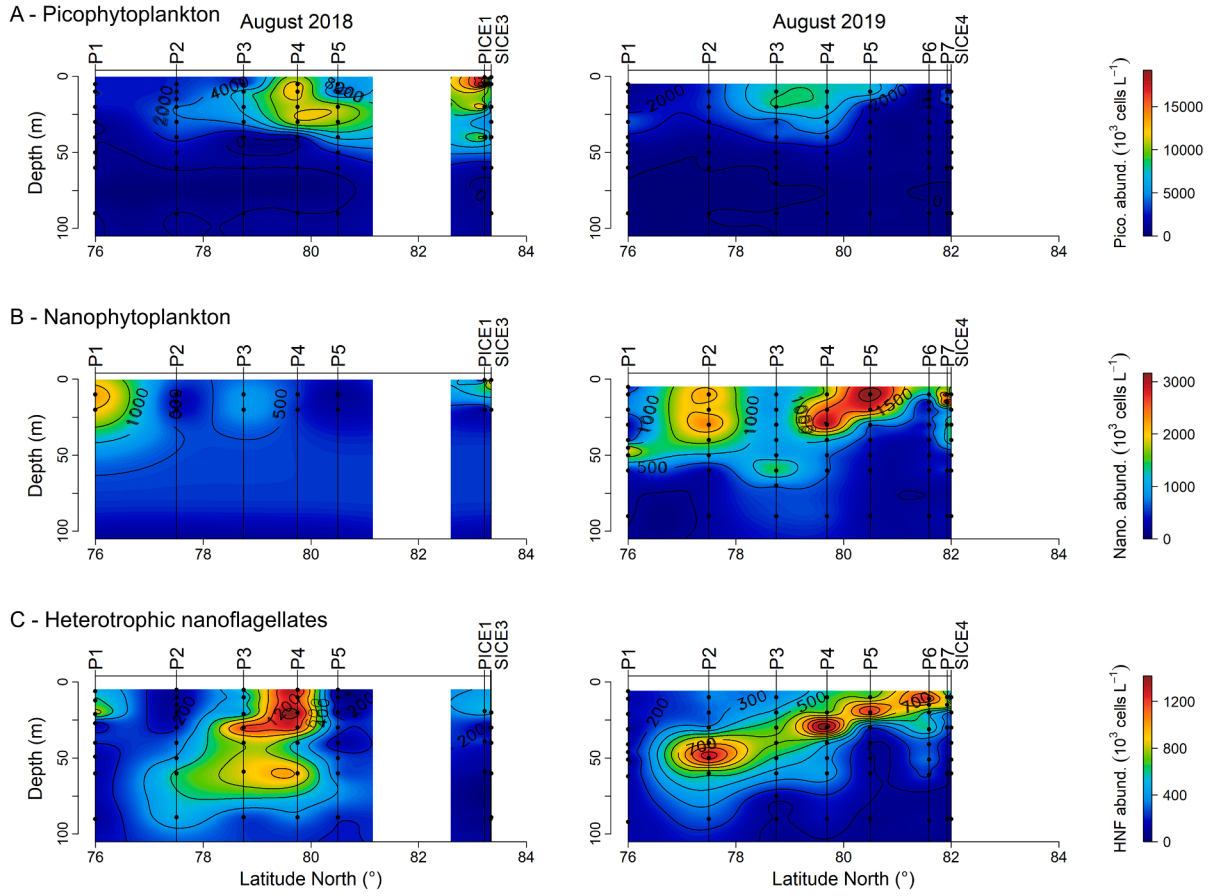

Fig. A6. Abundances (10^3 cells m^{-2}) of small phytoplankton (0.2–10 μm) along the sampling transects in the northwestern Barents Sea in 2018 (left panels) and 2019 (right panels) divided according to size into A) picophytoplankton, B) nanophytoplankton and C) heterotrophic nanoflagellates.

the higher chl *a* standing stocks in 2019. Indeed, satellites can underestimate Arctic Ocean primary production (based on satellite-derived chl *a*) by up to 40 % during the post-bloom period with a pronounced subsurface chl *a* maximum (Ardyna et al. 2017). The suggested higher chl *a* values in the coastal areas recorded from satellites in both years were likely an artefact caused by sediment-rich waters that interfere with the chl *a* retrieval algorithm (Blondeau-Patissier et al., 2014; Blix et al., 2018). However, this did not compromise the comparison of satellite-derived and *in situ* chl *a* observations as we were focusing on the more off-shore parts of the northwestern Barents Sea in this study.

In 2018, the protist community was dominated by small-sized autotrophic (Fig. 7) and heterotrophic protists, mainly flagellates and ciliates (Fig. 4), indicative of a late-summer oligotrophic state (see 4.2 and 4.3). This is in line with other studies investigating interannual variability in taxonomic compositions of planktonic communities (Wiktor and Wojciechowska, 2005; Kubiszyn et al., 2014; Hegseth et al., 2019; Dąbrowska et al., 2020, 2021; Dybwad et al., 2021; Assmy et al., 2023). In 2018, the relatively warm polar surface layer (>2.5 °C) extended further north (to at least station P5) and had a larger vertical extent (ca. 50 m) than in 2019, indicative of longer exposure to surface insolation. This was reflected in the deeper nutricline of nitrate, silicate and phosphate and much less pronounced subsurface chl *a* maxima in 2018 compared to 2019 (Fig. 2C–F). In 2019, the subsurface chl *a* maximum was clearly following the shoaling of the nutricline from south to north along the transect and was well within the euphotic zone (Fig. 2F). Although the euphotic zone extended to greater depths in 2018 due to lower particle concentrations and no sea-ice cover, except at the two northernmost ice stations (Fig. 2F), the deeper nutricline in 2018 likely limited phytoplankton growth. The water column at stations P1 and P2 south and north of the Polar Front showed similar nutrient concentrations in both years, likely due to the absence of sea ice over a longer period at these southernmost locations of the study area. There was no distinct surface low-salinity layer in 2018 compared to 2019 suggesting that wind events had likely mixed the surface layer although not sufficiently deep to entrain nutrients from sub-surface waters. The permanently open-water station P1 sustained higher late-summer protist standing stocks than meltwater-stratified previously ice-covered stations (P2 to P5 in 2018 and P2 to P4 in 2019) and likely showed less pronounced seasonality.

The more extensive ice cover in 2019 during the time of sampling (southern limit at ca. 79.8°N) resulted in a colder and fresher surface layer than in 2018. Autotrophic protists, including ice-associated taxa, had a higher contribution to protist standing stocks in August 2019, as suggested by the higher chl *a* concentrations compared to August 2018. In August 2019, chl *a* concentrations peaked at station P5 with 2.6 μg L^{-1}, indicating that the pelagic ecosystem was in a late-bloom situation. During the spring bloom chl *a* concentrations can reach up to 20 μg L^{-1} (Engelsen et al., 2002), while in summer, concentrations typically do not exceed 2 μg L^{-1} in Atlantic waters (Piwosz et al., 2009). In August 2018, chl *a* concentrations were very low (<0.5 μg L^{-1}), typical for summer conditions in the study area (Dalpadado et al., 2014). This was also reflected in 2–22-fold higher chl *a* standing stocks in 2019 (range from 34 – 67 mg chl *a* m^{-2}) compared to 2018 (range from 3 to 18 mg chl *a* m^{-2}).

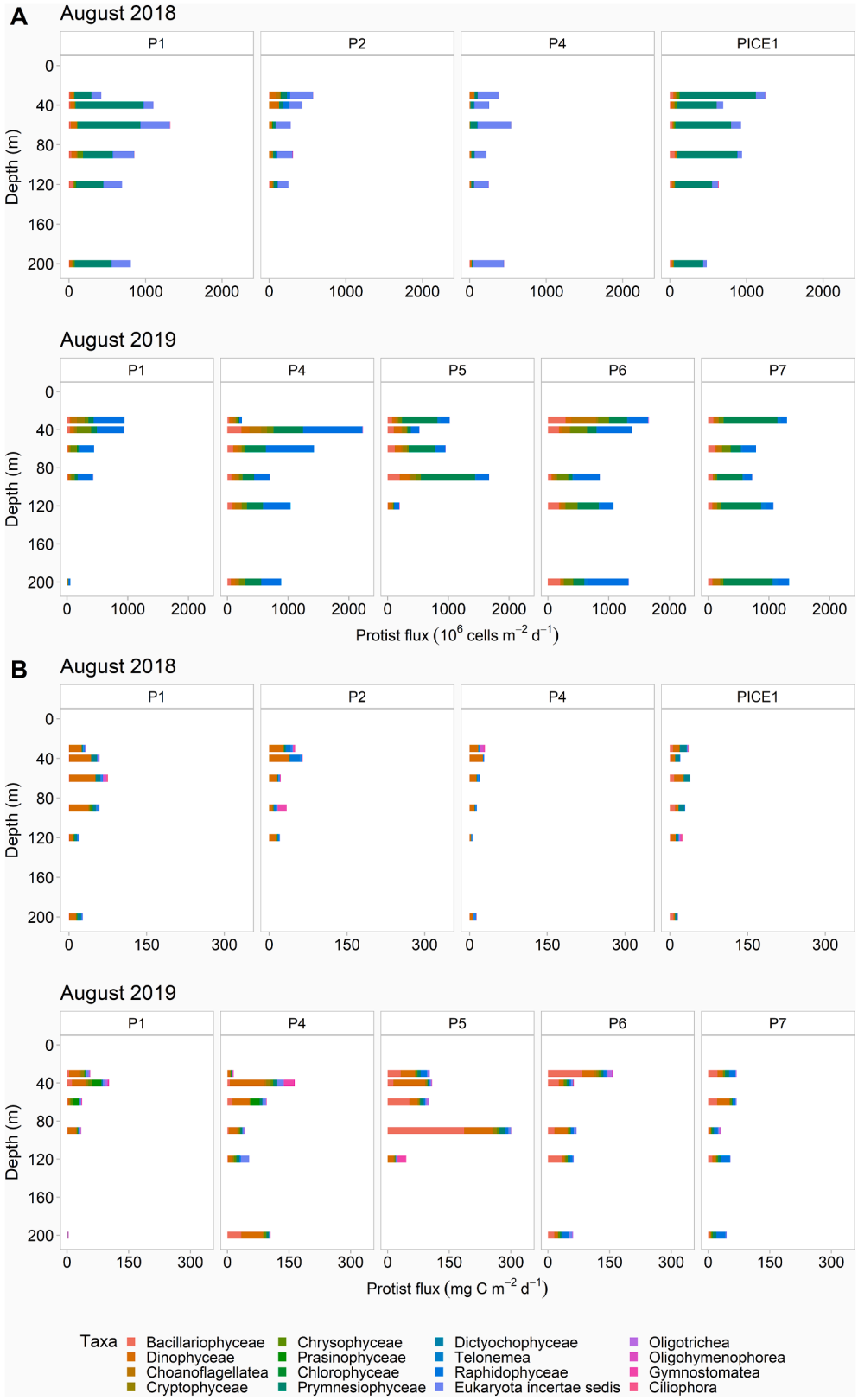

Fig. A7. Vertical flux of protist A) abundances (10^6 cells m^{-2} d^{-1}) and B) biomass (mg C m^{-2} d^{-1}) per depth (m) of all identified taxa along the sampling transects in the northwestern Barents Sea in August 2018 (top panels) and August 2019 (bottom panels). Note: data not available for all stations.

4.2. Differences in protist composition and consequences for vertical carbon flux

Diatoms had a higher contribution to protist standing stocks in 2019, which was in line with the shallower silicline as diatoms require a minimum of 2 µM to dominate phytoplankton communities (Egge and Aksnes, 1992). This can be largely attributed to the above-mentioned differences in seasonal succession stage linked to the onset of ice melt

Table A1
Sea-ice concentration and properties along the sampling transects in the northwestern Barents Sea in the two sampling years 2018 and 2019. Nd: data not available.

Station	Lat (°N)	Lon (°E)	Sea-ice concentration	Primary ice type	Ice thickness (cm)	Snow depth (cm)	Melt pond (tenths)
2018							
P1	75.9966	31.2299	0				
P2	77.5015	33.9962	0				
P3	78.7508	33.9978	0				
P4	79.6932	33.9961	0				
P5	80.5006	34.0064	0				
PICE1	83.3321	31.5402	8	FYI	100	1	3
SICE3	83.2321	25.6739	9	SYI	180	2	1
2019							
P1	76.0000	31.2194	0				
P2	77.5006	33.9865	0				
P3	78.7498	34.0008	0				
P4	79.6932	34.2300	6	FYI < 70 cm	nd	nd	nd
P5	80.5289	33.9602	8	FYI < 70 cm	nd	nd	nd
P6	81.585	31.5195	9	FYI < 70 cm	nd	nd	nd
P7	81.9262	29.1396	9	FYI < 70 cm	nd	nd	nd
SICE4	81.9957	24.9952	7	FYI < 70 cm	nd	nd	nd

Table A2
Descriptive statistics for estimated monthly chlorophyll (chl) *a* climatologies considering the area of interest (71° – 80° N latitude and 16° –52° E longitude).

Month	Mean chl *a*		Standard deviation		Variance	
	2018	2019	2018	2019	2018	2019
April	0.77	0.97	1.37	2.07	1.87	4.27
May	5.16	1.72	6.48	2.11	41.93	4.47
June	1.23	0.91	1.50	0.82	2.25	0.67
July	0.53	0.66	0.41	0.86	0.17	0.74
August	0.62	0.60	0.71	0.83	0.50	0.70
September	0.91	1.14	0.73	1.32	0.53	1.74

as diatom standing stocks were generally elevated at the ice-covered stations. It is interesting to note that in both years, diatom standing stocks were extremely low at open-water stations that were previously ice-covered, while at the permanently open-water station P1, diatom standing stocks were comparable to those in ice-covered waters. Diatoms showed the strongest relationship to sea ice at all locations, except for the permanently open-water station P1, suggesting strong ice-ocean feedbacks on nutrient and light availability *via* sea-ice meltwater stratification as well as snow and sea-ice light attenuation, respectively.

Species of the ice-associated diatom genus *Fragilariopsis* (Ratkova and Wassmann, 2002; Lundholm and Hasle, 2010; Szymanski and Gradinger, 2016), were found at high abundance near the ice edge (stations P4 and P5) in 2019 (Fig. A.4), while the centric diatom *Shionodiscus bioculatus* contributed a large share of diatom standing stocks at the northernmost ice stations in 2018 and 2019 (Fig. 6A). This species has been shown to accumulate in sea-ice ridges (Syvertsen 1991; Fernández-Méndez et al., 2018), hence its dominance in the water column likely reflects cryo-pelagic coupling caused by ice melt. The elevated vertical carbon flux of 296 mg C m^{-2} d^{-1} (station P5) observed in 2019 (Fig. 8B) was dominated by pelagic diatoms of the genus *Thalassiosira* and roughly 2-fold higher than the flux dominated by flagellates and dinoflagellates (<160 mg C m^{-2} d^{-1}). *Thalassiosira* species are known to dominate Arctic spring blooms (von Quillfeldt, 2000; Degerlund and Eilertsen, 2010; Hegseth et al., 2019; Assmy et al., 2023) and significantly contribute to vertical carbon flux (Rynearson et al., 2013; Dybwad et al., 2021) and were likely late remains of the preceding bloom. It needs to be noted that many of the dominant diatoms in both years were species with a relatively wide geographic distribution and are known to often occur later in the season, such as *Thalassiosira nordenskioeldii* (von Quillfeldt, 2000), *Chaetoceros debilis/curvisetus* (Tomas, 1997) and the *Rhizosolenia* species. The genus *Rhizosolenia* hosts large cylindrical species that have been associated with a shade flora growing at low light levels, likely facilitated by buoyancy regulation to allow them to migrate between the euphotic zone and the deep nutricline (Kemp et al., 2000).

Athecate dinoflagellates of the genus *Gymnodinium* made a large contribution to dinoflagellate standing stocks (Fig. 6B, Fig. A.5). This diverse but understudied genus (Kubiszyn and Wiktor, 2016) is known to include mixotrophic and heterotrophic species (Tomas, 1997; Stoecker and Lavrentyev, 2018). The obligatory heterotrophic dinoflagellate genus *Protoperidinium* was found predominantly at station P1 in 2018 and is known to feed on large diatoms *via* their pallium feeding mode (Jacobson and Anderson, 1986). The prominent role of dinoflagellates is also reflected in their high contribution to biomass flux (Fig. 8B).

Within the flagellate community, the prymnesiophyte *Phaeocystis pouchetii,* an important bloom former in the Atlantic sector of the Arctic (Degerlund and Eilertsen, 2010; Ardyna et al., 2020; Dąbrowska et al., 2020), sticks out with the highest abundances at the two northernmost ice-covered stations in 2018 (Fig. A.4), likely fuelled by the still elevated surface nutrient concentrations. This species often occurs at a later successional stage after the diatom spring bloom (von Quillfeldt, 2000; Hegseth et al., 2019), which is consistent with the generally low diatom biomass in 2018 (Fig. 4B). Deep mixing at station P1, indicated by elevated temperatures down to > 100 m, might have facilitated downward transport of *Phaeocystis* single cells, but overall, the carbon flux at station P1 and PICE1 was relatively low (<150 mg C m^{-2} d^{-1}). This is in agreement with previous vertical flux studies from the Barents Sea and north of Svalbard that have shown that a shift from a diatom to a *Phaeocystis* dominance could weaken the biological carbon pump (Wiedmann et al., 2020; Dybwad et al., 2021). The observed increase of *Phaeocystis pouchetii* in the Barents Sea (Orkney et al., 2020) could hence have a negative impact on strength of the biological carbon pump.

Altered temperature and seawater properties have further been suggested to favour the coccolithophore *Emiliania huxleyi* (Smyth et al., 2004; Giraudeau et al., 2016), which has shown a poleward expansion (Hegseth and Sundfjord, 2008; Winter et al., 2014; Oziel et al., 2017; Neukermans et al., 2018). Somewhat surprisingly, *E. huxleyi* contributed very little to protist biomass in 2018 and was virtually absent in 2019. The bloom of this species had likely been terminated by the time of sampling. Silkin et al. (2020) reported *E. huxleyi* blooms in the Barents Sea every summer between 2014 and 2018, typically being most prevalent in August (Signorini and McClain, 2009; Hovland et al., 2014). Our sampling stations, except P1, were likely located above its northernmost distribution limit, as this species is associated with Atlantic water masses (Silkin et al., 2020). This is supported by metabarcoding data which detected this species predominantly at station P1 in both years (B. Edvardsen, pers. comm.). Furthermore, it cannot be excluded that coccolithophores lost their scales, to some extent, during sample fixation and were consequently categorised as unidentified flagellates. Both *P. pouchetii* and *E. huxleyi* are predicted to increase in abundance and

Table A3
Overview of station presence of all identified protists from Niskin bottle samples collected during August 2018 and August 2019 in the northwestern Barents Sea.

Taxa	Class	Species	August 2018	August 2019	Carbon conversion factor (pg C cell^{-1})
Diatoms	Bacillariophyceae	*Attheya longicornis*	SICE3	P6, P7, SICE4	12
Diatoms	Bacillariophyceae	*Bacterosira bathyomphala*	P1, SICE3	P6	383
Diatoms	Bacillariophyceae	*Chaetoceros borealis*	P1, PICE1, SICE3	P4, P5, P6, P7, SICE4	403
Diatoms	Bacillariophyceae	*Chaetoceros* cf. *atlanticus*	SICE3		276
Diatoms	Bacillariophyceae	*Chaetoceros* cf. *borealis/convolutus/ concavicornis*	P1, P3		270
Diatoms	Bacillariophyceae	*Chaetoceros* cf. *borealis/eibenii*	P5		339
Diatoms	Bacillariophyceae	*Chaetoceros* cf. *convolutus/concavicornis*	PICE1, SICE3	P5, P7	204
Diatoms	Bacillariophyceae	*Chaetoceros* cf. *debilis/curvisetus*	PICE1	P6	208
Diatoms	Bacillariophyceae	*Chaetoceros concavicornis* f. *trisetosa*		P1, P7, SICE4	177
Diatoms	Bacillariophyceae	*Chaetoceros debilis*	PICE1, SICE3	SICE4	208
Diatoms	Bacillariophyceae	*Chaetoceros decipiens*	P3, PICE1, SICE3	P4, P6, P7, SICE4	563
Diatoms	Bacillariophyceae	*Chaetoceros furcellatus*	P2, PICE1, SICE3	P3, P5, P6, SICE4	24
Diatoms	Bacillariophyceae	*Chaetoceros gelidus* (formerly *C. socialis*)		P6, SICE4	21
Diatoms	Bacillariophyceae	*Chaetoceros laciniosus*		P3, P7, SICE4	144
Diatoms	Bacillariophyceae	*Chaetoceros similis*		P1, SICE4	102
Diatoms	Bacillariophyceae	*Chaetoceros* sp.	P1, PICE1, SICE3	P2	25
Diatoms	Bacillariophyceae	*Chaetoceros subtilis*		P1	27
Diatoms	Bacillariophyceae	*Chaetoceros tenuissimus*	SICE3	P6	6.0
Diatoms	Bacillariophyceae	*Chaetoceros teres*		SICE4	477
Diatoms	Bacillariophyceae	*Chaetoceros wighamii*	P4, PICE1	P7, SICE4	91
Diatoms	Bacillariophyceae	*Coscinodiscus* sp. 60–70 µm		P6, P7	7067
Diatoms	Bacillariophyceae	*Cylindrotheca closterium*	P1, P2, P5, PICE1, SICE3	P1, P3, P6, P7, SICE4	23
Diatoms	Bacillariophyceae	*Diploneis littoralis*	PICE1		413
Diatoms	Bacillariophyceae	*Entomoneis kjellmanii*	SICE3		951
Diatoms	Bacillariophyceae	*Eucampia groenlandica*	PICE1, SICE3	P4, P6, P7, SICE4	966
Diatoms	Bacillariophyceae	*Fragilariopsis* cf. *nana*		P1, P5	3.5
Diatoms	Bacillariophyceae	*Fragilariopsis cylindrus*	PICE1	P4, P5, P6, P7, SICE4	12
Diatoms	Bacillariophyceae	*Fragilariopsis nana*		P4, P5, P7	3.5
Diatoms	Bacillariophyceae	*Fragilariopsis oceanica*	PICE1	P7, SICE4	17
Diatoms	Bacillariophyceae	*Gyrosigma fasciola*	PICE1		801
Diatoms	Bacillariophyceae	*Lennoxia faveolata*		P3, P4, P7	3.0
Diatoms	Bacillariophyceae	*Leptocylindrus danicus*	P1, SICE3		95
Diatoms	Bacillariophyceae	*Leptocylindrus minimus*	P1	P1, SICE4	22
Diatoms	Bacillariophyceae	*Licmophora gracilis*	P1, P2, SICE3	P5	683
Diatoms	Bacillariophyceae	*Melosira arctica*	PICE1, SICE3		199
Diatoms	Bacillariophyceae	*Navicula* sp. 50–60 µm	PICE1		891
Diatoms	Bacillariophyceae	*Navicula directa*		P4, SICE4	549
Diatoms	Bacillariophyceae	*Navicula pelagica*	P5		109
Diatoms	Bacillariophyceae	*Navicula transitans*		P4, P6, P7, SICE4	127
Diatoms	Bacillariophyceae	*Nitzschia* 150–160 µm	SICE3		411
Diatoms	Bacillariophyceae	*Nitzschia* 50–60 µm		P6, SICE4	152
Diatoms	Bacillariophyceae	*Nitzschia* 70–80 µm	PICE1		207
Diatoms	Bacillariophyceae	*Nitzschia* 90–150 µm	P2		321
Diatoms	Bacillariophyceae	*Nitzschia frigida*	PICE1	P4, P6, P7, SICE4	29
Diatoms	Bacillariophyceae	*Nitzschia promare*	PICE1	SICE4	89
Diatoms	Bacillariophyceae	*Opephora* 60–70 µm		P6	279
Diatoms	Bacillariophyceae	*Pennales* 20–30 µm	P4, P5		13
Diatoms	Bacillariophyceae	*Pennales* 40–50 µm	P5	P7	65
Diatoms	Bacillariophyceae	*Pennales* 50–60 µm	PICE1		279
Diatoms	Bacillariophyceae	*Pleurosigma stuxbergii*	P1		539
Diatoms	Bacillariophyceae	*Porosira glacialis*		SICE4	3388
Diatoms	Bacillariophyceae	*Proboscia alata*		P1, P7, SICE4	1876
Diatoms	Bacillariophyceae	*Pseudo-nitzschia* cf. *delicatissima/ pseudodelicatissima*	P1, P2, PICE1, SICE3	P1, P4, P5, P6, P7, SICE4	18
Diatoms	Bacillariophyceae	*Pseudo-nitzschia* cf. *granii*		P1, SICE4	38
Diatoms	Bacillariophyceae	*Pseudo-nitzschia* cf. *pungens*	SICE3	P1	147
Diatoms	Bacillariophyceae	*Pseudo-nitzschia pungens*		SICE4	147
Diatoms	Bacillariophyceae	*Rhizosolenia hebetata* f. *hebetata*	P1, PICE1, SICE3	P1	1679
Diatoms	Bacillariophyceae	*Rhizosolenia hebetata* f. *semispina*	P1, PICE1, SICE3	P1, P6, P7, SICE4	1260
Diatoms	Bacillariophyceae	*Shionodiscus bioculatus* (formerly *Thalassiosira bioculata)*	PICE1, SICE3	P5, P6, P7, SICE4	2279
Diatoms	Bacillariophyceae	*Skeletonema* cf. *costatum*		P5, SICE4	33
Diatoms	Bacillariophyceae	*Skeletonema marinoi*		P3, P5	33
Diatoms	Bacillariophyceae	*Synedropsis hyperborea*	PICE1	P6, P7, SICE4	18
Diatoms	Bacillariophyceae	*Thalassiosira* 10–20 µm		P1, P2, P5, P7, SICE4	121
Diatoms	Bacillariophyceae	*Thalassiosira* 20–30 µm	P3, P5, PICE1	P1, P2, P4, P5, P6, P7, SICE4	340
Diatoms	Bacillariophyceae	*Thalassiosira* 30–40 µm	P1, P3, P5, PICE1	P7	770

(*continued on next page*)

Table A3 (*continued*)

Taxa	Class	Species	August 2018	August 2019	Carbon conversion factor (pg C cell^{-1})
Diatoms	Bacillariophyceae	*Shionodiscus bioculatus* var. *exigua* (formerly *Thalassiosira bioculata* var. *exigua*)	P1, SICE3	P7	2279
Diatoms	Bacillariophyceae	*Thalassiosira* cf. *gravida/antarctica*	P1, PICE1, SICE3	P1, P6, P7, SICE4	762
Diatoms	Bacillariophyceae	*Thalassiosira* cf. *pacifica/hyalina*		P4, P5	746
Diatoms	Bacillariophyceae	*Thalassiosira gravida*		P6	762
Diatoms	Bacillariophyceae	*Thalassiosira nordenskioeldii*	PICE1, SICE3	P4, P6, P7, SICE4	427
Dinoflagellates	Dinophyceae	*Alexandrium* 20–30 µm	SICE3	P1	1860
Dinoflagellates	Dinophyceae	*Alexandrium* 30–40 µm		P3, P7	2563
Dinoflagellates	Dinophyceae	*Amphidinium longum*	P1, P2, P3	P1, P2, P3, P4, P6, SICE4	189
Dinoflagellates	Dinophyceae	*Amphidinium sphenoides*	P2, P3, P4, P5, PICE1, SICE3	P1, P2, P5, P6, P7, SICE4	99
Dinoflagellates	Dinophyceae	*Amphidoma acuminata*	SICE3		52
Dinoflagellates	Dinophyceae	*Amylax triacantha*	P1, P3		815
Dinoflagellates	Dinophyceae	*Cochlodinium* 70–80 µm		SICE4	2925
Dinoflagellates	Dinophyceae	*Dicroerisma psilonereiella*	SICE3		126
Dinoflagellates	Dinophyceae	*Dinophyceae* 30–40 µm	PICE1		3832
Dinoflagellates	Dinophyceae	*Dinophysis acuta*	P1		6408
Dinoflagellates	Dinophyceae	*Gonyaulax spinifera*	P1, P5		2123
Dinoflagellates	Dinophyceae	Gymnodiniales indet.	P2		1849
Dinoflagellates	Dinophyceae	Gymnodiniales indet. 10–20 µm	P5		130
Dinoflagellates	Dinophyceae	Gymnodiniales indet. 20–30 µm	P1, P2, P3, P5	P2, P4, P6, SICE4	484
Dinoflagellates	Dinophyceae	Gymnodiniales indet. 30–40 µm	P3	P1, P3, SICE4	1223
Dinoflagellates	Dinophyceae	Gymnodiniales indet. 40–50 µm	P3, PICE1	P2	2243
Dinoflagellates	Dinophyceae	Gymnodiniales indet. 50–60 µm		P6	2802
Dinoflagellates	Dinophyceae	*Gymnodinium* 5–10 µm	P1, P2, P3, P4, P5, SICE3	P4, P5, P6, P7	49
Dinoflagellates	Dinophyceae	*Gymnodinium* 10–20 µm	P1, P2, P3, P4, P5, PICE1, SICE3	P1, P2, P3, P4, P5, P6, P7, SICE4	130
Dinoflagellates	Dinophyceae	*Gymnodinium* 20–30 µm	P1, P2, P3, P5, PICE1, SICE3	P1, P2, P5, P7, SICE4	484
Dinoflagellates	Dinophyceae	*Gymnodinium arcticum*	P5, PICE1	P6, SICE4	121
Dinoflagellates	Dinophyceae	*Gymnodinium* cf. *filum*	SICE3		1956
Dinoflagellates	Dinophyceae	*Gymnodinium galeatum*	P1, P2, P3, P4, P5, PICE1, SICE3	P1, P2, P3, P4, P5, P6, P7, SICE4	266
Dinoflagellates	Dinophyceae	*Gymnodinium gracilentum*	P1, P2, P3, P4, P5, PICE1	P1, P2, P3, P4, P7, SICE4	266
Dinoflagellates	Dinophyceae	*Gymnodinium ostenfeldii* 10–20 µm	PICE1		57
Dinoflagellates	Dinophyceae	*Gymnodinium*	P1, P2, P5	P5, P6, SICE4	1849
Dinoflagellates	Dinophyceae	*Gymnodinium wulffii*	P1, P2, P3, P4, P5, PICE1, SICE3	P1, P3, P5, P6, P7, SICE4	182
Dinoflagellates	Dinophyceae	*Gyrodinium*	P3		2567
Dinoflagellates	Dinophyceae	*Gyrodinium* 10–20 µm	P2	P1, SICE4	91
Dinoflagellates	Dinophyceae	*Gyrodinium* 20–30 µm	P1, P2, P3, P4, P5, PICE1	P3, P6, P7	432
Dinoflagellates	Dinophyceae	*Gyrodinium* cf. *fusiforme* 20–30 µm	P2		2487
Dinoflagellates	Dinophyceae	*Gyrodinium* 30–40 µm	P1, P2, P3, P4, P5, PICE1	P2, P4, P5, P6	1164
Dinoflagellates	Dinophyceae	*Gyrodinium* 40–50 µm	P3	P5, SICE4	2243
Dinoflagellates	Dinophyceae	*Gyrodinium* 50–60 µm	P4, PICE1	P3	2802
Dinoflagellates	Dinophyceae	*Gyrodinium* 60–70 µm	SICE3		5751
Dinoflagellates	Dinophyceae	*Gyrodinium* cf. *gravida/antarctica*	P5		826
Dinoflagellates	Dinophyceae	*Gyrodinium* cf. *pepo*	P1		2567
Dinoflagellates	Dinophyceae	*Gyrodinium flagellare*	P5	P2, P3, P4, P5, P6, P7, SICE4	8
Dinoflagellates	Dinophyceae	*Gyrodinium fusiforme*	P1, P2, P3, P4, P5, PICE1, SICE3	P2, P3, P4, P5, P6, P7, SICE4	2429
Dinoflagellates	Dinophyceae	*Gyrodinium grave*	P1, P2, P3, SICE3	P2, P3, P6, P7, SICE4	2567
Dinoflagellates	Dinophyceae	*Gyrodinium spirale*	P1, P3, P5, PICE1	P1, P2, P3, P4, P6, P7, SICE4	4392
Dinoflagellates	Dinophyceae	*Heterocapsa* 30–40 µm		SICE4	856
Dinoflagellates	Dinophyceae	*Heterocapsa rotundata*	P2, P3, SICE3	P1, P2, P3, P4, P6, P7	36
Dinoflagellates	Dinophyceae	*Heterocapsa* sp.		P6	178
Dinoflagellates	Dinophyceae	*Heterocapsa triquetra*		P2, P5	225
Dinoflagellates	Dinophyceae	*Lebouridinium glaucum*	P1, P2, P3, P4, P5, PICE1, SICE3	P1, P2, P3, P5, P6, P7, SICE4	439
Dinoflagellates	Dinophyceae	*Lessardia elongata*	SICE3	P1, P4, P6, P7, SICE4	166
Dinoflagellates	Dinophyceae	*Micracanthodinium claytonii*	P2, P5, PICE1, SICE3	P1, P2, P3, P4, P6, P7, SICE4	546
Dinoflagellates	Dinophyceae	*Nematopsides vigilans*		P4, P6, SICE4	499
Dinoflagellates	Dinophyceae	Peridiniales	P1, P2		1900
Dinoflagellates	Dinophyceae	Peridiniales 10–20 µm	P1, P2, P3, P4, P5, PICE1, SICE3	P2, P3, P4, P5, P6, P7, SICE4	128

(*continued on next page*)

Table A3 (*continued*)

Taxa	Class	Species	August 2018	August 2019	Carbon conversion factor (pg C cell^{-1})
Dinoflagellates	Dinophyceae	Peridiniales 20–30 µm	P1, P2, P3, P4, P5, PICE1, SICE3	P1, P2, P3, P4, P5, P6, P7, SICE4	506
Dinoflagellates	Dinophyceae	Peridiniales 30–40 µm	P1, P2, P4	P1, P3, P6	950
Dinoflagellates	Dinophyceae	*Phalacroma rotundatum* (formerly *Dinophysis rotundata*)	P1	P1, P4, P5, SICE4	2479
Dinoflagellates	Dinophyceae	*Polarella glacialis*	P1	P3, P4, P7, SICE4	51
Dinoflagellates	Dinophyceae	*Pronoctiluca pelagica*	P1, P3, P4, PICE1, SICE3	P3, P5, P7, SICE4	297
Dinoflagellates	Dinophyceae	*Prorocentrum cordatum*	P1, P2, P3, P5, PICE1	P1, P3, P4, P5, P6, SICE4	173
Dinoflagellates	Dinophyceae	*Protoperidinium*	P1, P3		6473
Dinoflagellates	Dinophyceae	*Protoperidinium* 20–30 µm	P1	P7	517
Dinoflagellates	Dinophyceae	*Protoperidinium* 30–40 µm	P1, P3		1383
Dinoflagellates	Dinophyceae	*Protoperidinium* 40–50 µm	P1		2867
Dinoflagellates	Dinophyceae	*Protoperidinium* 50–60 µm	P1		5116
Dinoflagellates	Dinophyceae	*Protoperidinium bipes*	P1, P3, SICE3	P1, P4, P5, P7, SICE4	172
Dinoflagellates	Dinophyceae	*Protoperidinium brevipes*	P1, SICE3	P1, P4, P6	1286
Dinoflagellates	Dinophyceae	*Protoperidinium cerasus*	P3, SICE3	P1	3380
Dinoflagellates	Dinophyceae	*Protoperidinium* cf. *depressum/oceanica*	P1		12,388
Dinoflagellates	Dinophyceae	*Protoperidinium depressum*	P1		12,388
Dinoflagellates	Dinophyceae	*Protoperidinium islandicum*		P1	3116
Dinoflagellates	Dinophyceae	*Protoperidinium oceanicum*		P1	12,388
Dinoflagellates	Dinophyceae	*Protoperidinium pallidum*	P1	P1, P6	9764
Dinoflagellates	Dinophyceae	*Protoperidinium pellucidum*	P1, P2, P5, SICE3	P1, P6, P7, SICE4	3273
Dinoflagellates	Dinophyceae	*Protoperidinium pyriforme*	P1	P6	3380
Dinoflagellates	Dinophyceae	*Scrippsiella trochoidea*	P1, P4	P1, P6	695
Dinoflagellates	Dinophyceae	*Torodinium robustum*	P1, P2, P3, PICE1, SICE3	P1, P2, P4, P5, SICE4	569
Dinoflagellates	Dinophyceae	*Tripos arcticus* (formerly *Ceratium arcticum*)	P1	P1, P2	8128
Dinoflagellates	Dinophyceae	*Tripos fusus*	P1		2058
	Chlorodendrophyceae	*Pachysphaera pelagica*	P1, SICE3	P2, P4, P5, P7	63
Other flagellates	Chlorophyceae	*Chlamydomonas* sp.		P1, P5, P7	71
Other flagellates	Choanoflagellatea	*Bicosta spinifera*		P3, P4, P6, SICE4	5.1
Other flagellates	Choanoflagellatea	*Calliacantha natans*		P1, P2, P3, P4, P5, P7, SICE4	39
Other flagellates	Choanoflagellatea	*Monosiga marina*	P5, PICE1, SICE3	P2, P3, P4, P5, P6, P7, SICE4	9
Other flagellates	Choanoflagellatea	*Salpingoeca inquillata*		P2, P4, P7	10
Other flagellates	Chrysophyceae	Chrysophyceae sp.	P3	P2, P3, P4, P5, P6, P7, SICE4	77
Other flagellates	Chrysophyceae	*Dinobryon balticum*	P1, P2, P3, P4, P5, PICE1, SICE3	P1, P2, P3, P4, P6, P7, SICE4	18
Other flagellates	Chrysophyceae	*Dinobryon faculiferum*		P1, P3, P5, P6, P7, SICE4	11
Other flagellates	Chrysophyceae	*Dinobryon* sp.		P1, P5, P6, P7, SICE4	20
Other flagellates	Chrysophyceae	*Ochromonas* sp.	PICE1		7.0
Other flagellates	Cryptophyceae	Cryptophyceae indet.	P1, P2, P3, P5, SICE3	P1, P2, P3, P4, P5, P6, P7, SICE4	34
Other flagellates	Cryptophyceae	*Leucocryptos marina*	P1, P2, P3, P4, P5, PICE1, SICE3	P1, P2, P3, P4, P5, P6, P7, SICE4	24
Other flagellates	Cryptophyceae	*Plagioselmis prolonga*	P5	P2, P4, P7	10
Other flagellates	Cryptophyceae	*Rhodomonas* sp.		P5, SICE4	16
Other flagellates	Cryptophyceae	*Teleaulax amphioxeia*		P2	21
Other flagellates	Cryptophyceae	*Teleaulax* sp.	P2, SICE3	P2, P3, P4, P5, P6, P7, SICE4	27
Other flagellates	Dictyochophyceae	*Apedinella radians*	P1, P3	P1, P3, P6, SICE4	50
Other flagellates	Dictyochophyceae	*Octactis speculum* (formerly *Dictyocha speculum*)	P1, PICE1, SICE3	P3, P4, P5, P6, P7, SICE4	461
Other flagellates	Dictyochophyceae	*Pseudopedinella pyriformis*		P4	30
Other flagellates	Euglenoidea	Euglenoidea indet.	P4	P4, P7	233
Other flagellates	Euglenoidea	*Eutreptiella* sp.		P7	489
Other flagellates	Eukaryota incertae sedis	Flagellates indet.	PICE1, SICE3	P2	67

(*continued on next page*)

Table A3 (*continued*)

Taxa	Class	Species	August 2018	August 2019	Carbon conversion factor (pg C cell^{-1})
Other flagellates	Eukaryota incertae sedis	Flagellates indet. 0–3 µm	PICE1		1.2
Other flagellates	Eukaryota incertae sedis	Flagellates indet. 3–7 µm	P1, P2, P3, P4, P5, PICE1, SICE3	P1, P2, P3, P4, P5, P6, P7, SICE4	10
Other flagellates	Eukaryota incertae sedis	Flagellates indet. 7–10 µm	P1, P2, P5, PICE1, SICE3	P1, P2, P3, P5, P6, P7, SICE4	39
Other flagellates	Eukaryota incertae sedis	Flagellates indet. 10–20 µm	P5, PICE1	P2, P3, P5, P6, SICE4	205
Other flagellates	Pyramimonadophyceae	*Halosphaera* sp.		P5, SICE4	40
Other flagellates	Prasinophyceae	*Pterosperma*	P1		6005
Other flagellates	Prasinophyceae	*Pterosperma parallelum*		P1	6005
Other flagellates	Pyramimonadophyceae	*Pyramimonas nansenii*	SICE3	P7	4.2
Other flagellates	Pyramimonadophyceae	*Pyramimonas virginica*		P2, P4, P6	4.6
Other flagellates	Prymnesiophyceae	*Chrysochromulina* spp.	P2, P5, PICE1	P2, P3, P6, P7	38
Other flagellates	Prymnesiophyceae	*Phaeocystis pouchetii*	P1, P2, P4, PICE1, SICE3	P4, P5, P6, P7, SICE4	9.4
Other flagellates	Prymnesiophyceae	Prymnesiophyceae 10–20 µm		P3	62
Other flagellates	Prymnesiophyceae	*Pyramimonas* cf. *virginica*		P6	4.6
Other flagellates	Prymnesiophyceae	*Pyramimonas* sp.	P1, SICE3	P2, P4, P5, P7, SICE4	82
Other flagellates	Raphidophyceae	*Commation cryoporinum*		SICE4	8.0
Other flagellates	Raphidophyceae	*Heterosigma* sp.	P2, P3	P1, P2, P6, P7, SICE4	242
Other flagellates	Telonemea	*Telonema subtile*	PICE1	P2, P6, P7	7.9
Other flagellates	Xanthophyceae	*Meringosphaera mediterranea*		P2, P3	89
Ciliates	Ciliophora	Ciliophora		P3	245
Ciliates	Ciliophora	Ciliophora 30–40 µm	P1, P2, P4	P5, P7	1072
Ciliates	Ciliophora	Ciliophora 40–50 µm	P1	P5	1135
Ciliates	Ciliophora	Ciliophora 50–60 µm	P1		1298
Ciliates	Ciliophora	Ciliophora 60–70 µm	P1, P3		1661
Ciliates	Ciliophora	Ciliophora 70–80 µm	P1		1924
Ciliates	Ciliophora	Ciliophora 80–90 µm	P1, P5		2910
Ciliates	Gymnostomatea	*Didinium gargantua*		P2, P7, SICE4	4048
Ciliates	Gymnostomatea	*Didinium* sp.	P5, PICE1, SICE3	P2	4171
Ciliates	Gymnostomatea	*Mesodinium rubrum*	P1, P2, P3, P4, P5, PICE1, SICE3	P3, P4, P5, P6, P7, SICE4	3248
Ciliates	Gymnostomatea	*Mesodinium rubrum* 40–50 µm	P1		3248
Ciliates	Hypotrichea	*Euplotes* sp.		P6	966
Ciliates	Oligohymenophorea	*Scuticociliatia* indet. 10–20 µm	P3		532
Ciliates	Oligohymenophorea	*Scuticociliatia* indet.	P1, P2, P3, P5, PICE1	P2, P3, P6, P7, SICE4	532
Ciliates	Oligotrichea	*Acanthostomella norvegica*	P2, P3	P2, P3, P4, P5, P6, P7, SICE4	312
Ciliates	Oligotrichea	*Laboea strobila*	P1, P2, P3, P4, P5, SICE3	P1, P2, P3, P4, P6	2711
Ciliates	Oligotrichea	*Leegaardiella ovalis*	P1, P3, P5, PICE1, SICE3	P2, P5, SICE4	672
Ciliates	Oligotrichea	*Leegaardiella sol*	P1	SICE4	456
Ciliates	Oligotrichea	*Leprotintinnus* sp.	P1, P3		1660
Ciliates	Oligotrichea	*Lohmanniella oviformis*	P1, P2, P3, P4, P5, PICE1	P2, P3, P4, P5, P6, P7, SICE4	204
Ciliates	Oligotrichea	*Lohmanniella oviformis* 20–30 µm	P2		204
Ciliates	Oligotrichea	*Parafavella gigantea*	P5, SICE3		28,883
Ciliates	Oligotrichea	*Parafavella obtusangula*	P1	P1, P3	26,503
Ciliates	Oligotrichea	*Paratontonia gracillima*		P4, P7	1660
Ciliates	Oligotrichea	*Ptychocylis obtusa*	P1, P2, P3, P5	P2, P3, P4, P6, P7, SICE4	1660
Ciliates	Oligotrichea	*Salpingella secata*	P1		1660
Ciliates	Oligotrichea	*Strobilidium striatum*		P7	1072
Ciliates	Oligotrichea	*Strombidium*	P2, PICE1	P2, P6, P7	1010
Ciliates	Oligotrichea	*Strombidium* 10–20 µm	P2, P4, PICE1, SICE3	P2, P6, P7	185
Ciliates	Oligotrichea	*Strombidium* 20–30 µm	P1, P2, P3, P4, P5, PICE1, SICE3	P2, P3, P4, P5, P6, P7, SICE4	779
Ciliates	Oligotrichea	*Strombidium* 30–40 µm	P1, P2, P3, P4, P5, PICE1, SICE3	P2, P3, P6, P7, SICE4	2009

(*continued on next page*)

Table A3 (*continued*)

Taxa	Class	Species	August 2018	August 2019	Carbon conversion factor (pg C cell^{-1})
Ciliates	Oligotrichea	*Strombidium* cf. *acutum* 30–40 µm	P1		2009
Ciliates	Oligotrichea	*Strombidium* 40–50 µm	P1, P2, P3, P5		4077
Ciliates	Oligotrichea	*Strombidium* 50–60 µm	P3		7176
Ciliates	Oligotrichea	*Strombidium* 60–70 µm	P1, P2	P7	11,488
Ciliates	Oligotrichea	*Strombidium* cf. *acutum*	P1, P2, P3		2009
Ciliates	Oligotrichea	*Strombidium* cf. *scutellum*	P3		2009
Ciliates	Oligotrichea	*Strombidium* cf. *sulcatum*	P5, SICE3	P4, P5, P6	4077
Ciliates	Oligotrichea	*Strombidium* cf. *sulcatum/vestitum*		P6	2762
Ciliates	Oligotrichea	*Strombidium* cf. *vestitum*	P4, P5	P2	1403
Ciliates	Oligotrichea	*Strombidium conicum*	P1, P2, P3, P4, P5, PICE1, SICE3	P1, P2, P3, P4, P5, P6, P7, SICE4	11,170
Ciliates	Oligotrichea	*Strombidium constrictum*	P1, P3, P4, P5, SICE3	P1, P2, P3, P4, P6, P7, SICE4	6377
Ciliates	Oligotrichea	*Tintinnus inquilinus*	P1, P2, P5	P1	1660
Ciliates	Prostomatea	*Balanion comatum*	P1		245
Ciliates	Prostomatea	*Prorodon ovum*	P1		2910

extend poleward as a result of Atlantification (Neukermans et al., 2018; Orkney et al., 2020).

The dominance of *Dinobryon*, *Heterosigma* and *Chrysochromulina* at the other stations both in 2018 and 2019 (Fig. 6C) can likely be explained by their mixotrophic feeding mode, which will give them a competitive advantage in the oligotrophic surface layer since they can supplement their diet by feeding on bacteria, which has not been shown for *Phaeocystis*. Indeed, under-ice blooms of *Chrysochromulina* under low nutrient conditions have been attributed to mixotrophy (Søgaard et al., 2021) and *Dinobryon* is known to thrive under low nutrient and light conditions late in the season (McKenrie et al., 1995; Hegseth et al., 2019). The kleptoplastidic ciliates *Strombidium* and *Mesodinium rubrum*, which keep the plastids of their prey for a while to perform photosynthesis, dominated ciliate standing stocks (Fig. 6D), supporting the general finding that mixotrophy is a prominent trophic mode in the Arctic Ocean, especially during summer (Stoecker and Lavrentyev, 2018). Interestingly, at open water station P1, in both 2018 and 2019, protist standing stocks were among the highest, particularly if flagellates are excluded, but abundances of ciliates and dinoflagellates were rather low, illustrating that particularly large taxa, such as thecate dinoflagellates of the genus *Protoperidinium* and tintinnid ciliates of the genus *Parafavella*, were largely restricted to this open water station. Overall, it can be concluded that the relative contribution of heterotrophic and mixotrophic protists to total protist standing stocks was higher in 2018 than in 2019, reflecting the more oligotrophic status and more advanced successional stage of the protist community in August 2018. This is also confirmed by the higher contribution of protist carbon flux to total POC fluxes in 2019 compared to 2018, suggesting that vertical flux in 2018 had a higher share of regenerated material and detritus.

4.3. Relationship between protist size structure and nutrient concentrations

The most pronounced differences in the protist communities between the late summers were observed for nanophytoplankton. Its biomass was considerably higher in August 2019 than in August 2018 (Fig. 7B), reflected in the higher chl *a* standing stocks in 2019. Indeed, much of the difference in chl *a* standing stocks can likely be explained by this group as the interannual differences in larger protists identified under light microscopy were less pronounced, also indicating that nanoplanktonic protists were likely not fully captured by the latter method. This is further supported by the close match of nanophytoplankton biomass, as measured by flow cytometry, and the subsurface chl *a* maximum in both years. This match with the subsurface chl *a* maximum was particularly evident for the larger of the two nanophytoplankton size fractions (5–10 µm; data not shown), indicating a close association with the nutricline. Biomass of the smaller nanophytoplankton size fraction (2–5 µm) and picophytoplankton (Fig. 7A) on the other hand showed an inverse pattern with chl *a* concentrations and were generally most abundant where nutrient concentrations were the lowest. The biomass of HNF largely matched the subsurface chl *a* maximum (Fig. 7C), particularly in 2019, suggesting active feeding on smaller phytoplankton. However, they also matched the abundance of large bacteria (Amargant-Arumí et al. in prep., same issue), which was likely their main food source since HNF are major consumers of bacteria in the ocean (Sherr et al., 1997; Kopylov et al., 2016). Thus, the most likely scenario is that elevated levels of labile organic carbon in the subsurface chl *a* maximum sustained bacterial growth, which again supported their HNF grazers.

In the context of environmental change, the sea-ice conditions and consequently protist community structure in the northwestern Barents Sea during 2018 can give us a glimpse into the future when the Barents Sea is predicted to be sea-ice free during the summer (Onarheim and Årthun, 2017; Serreze and Meier, 2019), and longer open-water periods are likely to ultimately favour mixo- and heterotrophic flagellates and their protozoan grazers due to higher surface temperatures and decreased nutrient availability as outlined in Fig. 9. It is suggested that small-celled species, covering pico- and smaller nanophytoplankton fractions, will benefit from oligotrophic environments with longer open-water seasons (Nöthig et al., 2015; Zhang et al., 2015; Wang et al., 2019) as they can adapt to low nutrient conditions (Zhang et al., 2016) due to their larger surface-to-volume-ratio and thus superior nutrient uptake capability (Litchman et al., 2007). In comparison to e.g. (large-celled) diatoms, which are in the preferred prey-size class of *Calanus* copepods (Mullin, 1963), an essential link between primary production and higher trophic levels, smaller cells are suboptimal for efficient grazing by mesozooplankton (Levinsen et al., 2000; Kiørboe, 2011). While picophytoplankton is significant for the ocean's carbon cycle (Buitenhuis et al., 2012; Richardson, 2019), changes in protist community composition with the warming of the ocean are expected to have direct consequences for copepod grazers and the associated food web (Li et al., 2009; Finkel et al., 2010; Dąbrowska et al., 2020; Thingstad, 2020).

5. Conclusions

Our study shows interannual variability in summer protist communities during two years with contrasting sea-ice conditions in the northwestern Barents Sea. The environmental conditions encountered in August 2018 are likely representative of the future Barents Sea, with earlier sea-ice melt and a longer open water season (Onarheim and Årthun, 2017). Annual primary production in the Arctic Ocean has been shown to increase as a result of a longer open water season (Arrigo and van Dijken, 2015), and these changes in the physical

Table A4
Overview of all identified species of sinking protists from sediment trap deployments collected during August 2018 and August 2019 in the Barents Sea. *species not observed in sediment trap samples.

Taxa	Class	Species	August 2018	August 2019	Carbon conversion factor (pg C cell^{-1})
Diatoms	Bacillariophyceae	*Actinocyclus* sp.*		P4	2460
Diatoms	Bacillariophyceae	*Actinocyclus tenuissimus**		P4	1794
Diatoms	Bacillariophyceae	*Attheya septentrionalis**	P1, PICE1	P5, P6	82
Diatoms	Bacillariophyceae	*Bacterosira bathyomphala*	PICE1	P6, P7	383
Diatoms	Bacillariophyceae	*Chaetoceros borealis*		P4, P5, P6, P7	403
Diatoms	Bacillariophyceae	*Chaetoceros concavicornis*	PICE1	P5, P6	177
Diatoms	Bacillariophyceae	*Chaetoceros convolutus*		P1, P7	231
Diatoms	Bacillariophyceae	*Chaetoceros decipiens*	PICE1	P6, P7	563
Diatoms	Bacillariophyceae	*Chaetoceros furcellatus*	P2, P4, PICE1	P4, P5, P6, P7	24
Diatoms	Bacillariophyceae	*Chaetoceros gelidus* (formerly *C. socialis*)	PICE1	P6, P7	21
Diatoms	Bacillariophyceae	*Chaetoceros laciniosus*	PICE1		144
Diatoms	Bacillariophyceae	*Chaetoceros* sp.	PICE1	P1	25
Diatoms	Bacillariophyceae	*Chaetoceros tenuissimus*	P1, P2, PICE1	P1, P4, P5, P6, P7	6.0
Diatoms	Bacillariophyceae	*Coscinodiscus centralis**		P5	36,320
Diatoms	Bacillariophyceae	*Coscinodiscus* sp.		P5, P6, P7	7067
Diatoms	Bacillariophyceae	*Cylindrotheca closterium*	P1, P2, PICE1	P1, P4, P5, P7	23
Diatoms	Bacillariophyceae	*Eucampia groenlandica*	PICE1	P4, P5, P6, P7	966
Diatoms	Bacillariophyceae	*Fragilariopsis cylindrus*	P1, PICE1	P1, P4, P5, P6, P7	12
Diatoms	Bacillariophyceae	*Fragilariopsis nana*		P4	3.5
Diatoms	Bacillariophyceae	*Fragilariopsis oceanica*	PICE1	P4	17
Diatoms	Bacillariophyceae	*Lauderia annulata**		P7	1257
Diatoms	Bacillariophyceae	*Navicula pelagica*	PICE1	P4, P5, P6	109
Diatoms	Bacillariophyceae	*Navicula septentrionalis**		P5	87
Diatoms	Bacillariophyceae	*Navicula* sp.		P6	260
Diatoms	Bacillariophyceae	*Navicula transitans*		P6	127
Diatoms	Bacillariophyceae	*Navicula vanhoeffenii**		P4	77
Diatoms	Bacillariophyceae	*Nitzschia frigida*	PICE1	P4, P5, P6	29
Diatoms	Bacillariophyceae	*Nitzschia longissima**	P1		28
Diatoms	Bacillariophyceae	*Pauliella taeniata**	PICE1		69
Diatoms	Bacillariophyceae	*Pleurosigma* sp.		P4	539
Diatoms	Bacillariophyceae	*Porosira glacialis*		P6	3388
Diatoms	Bacillariophyceae	*Pseudo-nitzschia* cf. *delicatissima/pseudodelicatissima*	P1, PICE1	P1, P5, P6, P7	18
Diatoms	Bacillariophyceae	*Pseudo-nitzschia granii*	P1, PICE1	P1, P4, P5, P7	38
Diatoms	Bacillariophyceae	*Pseudo-nitzschia seriata**		P1	268
Diatoms	Bacillariophyceae	*Rhizosolenia hebetata* f. *hebetata*	P1, PICE1	P1, P5, P6, P7	1679
Diatoms	Bacillariophyceae	*Rhizosolenia hebetata* f. *semispina*		P1	1260
Diatoms	Bacillariophyceae	*Skeletonema costatum*		P5	33
Diatoms	Bacillariophyceae	*Synedropsis hyperborea*	PICE1	P1, P5, P6, P7	18
Diatoms	Bacillariophyceae	*Thalassiosira* 20–30 μm		P4	340
Diatoms	Bacillariophyceae	*Shionodiscus bioculatus* (formerly *Thalassiosira bioculata)*	PICE1	P1, P5, P6, P7	2279
Diatoms	Bacillariophyceae	*Thalassiosira* cf. *gravida/antarctica*	PICE1	P1, P4, P5, P6, P7	762
Diatoms	Bacillariophyceae	*Thalassiosira* cf. *weissflogii**		P5, P6, P7	159
Diatoms	Bacillariophyceae	*Thalassiosira hyalina**		P6, P7	746
Diatoms	Bacillariophyceae	*Thalassiosira nordenskioeldii*	PICE1	P5, P6, P7	427
Diatoms	Bacillariophyceae	*Trachyneis* sp.*		P4	260
Dinoflagellates	Dinophyceae	*Alexandrium* sp.	P1, P2, P4, PICE1	P1, P4, P5	1301
Dinoflagellates	Dinophyceae	*Amphidinium longum*		P4	189
Dinoflagellates	Dinophyceae	*Amphidinium sphenoides*	P1, P2	P6	99
Dinoflagellates	Dinophyceae	*Cochlodinium* sp.	P2	P4, P5, P6, P7	2814
Dinoflagellates	Dinophyceae	*Dicroerisma psilonereiella*		P5	126
Dinoflagellates	Dinophyceae	Dinophyceae 10–20 μm	P2		373
Dinoflagellates	Dinophyceae	*Dinophyceae* indet.	P1, P2	P1, P4, P7	2380
Dinoflagellates	Dinophyceae	*Dinophysis acuminata**		P4	1921
Dinoflagellates	Dinophyceae	*Dinophysis norvegica**	P1	P1	4693
Dinoflagellates	Dinophyceae	*Gonyaulax gracilis**	P1, P4, PICE1	P5	4880
Dinoflagellates	Dinophyceae	*Gonyaulax* sp.		P1, P4	4880
Dinoflagellates	Dinophyceae	Gymnodiniales 10–20 μm	P1, P2, P4, PICE1	P1, P4, P5, P6, P7	130
Dinoflagellates	Dinophyceae	Gymnodiniales 20–30 μm	P1	P1, P4, P5, P6, P7	484
Dinoflagellates	Dinophyceae	*Gymnodinium*	PICE1		1849
Dinoflagellates	Dinophyceae	*Gymnodinium* 10–20 μm	P2	P4, P5	130
Dinoflagellates	Dinophyceae	*Gymnodinium* cf. *arcticum*	P2, P4, PICE1	P1, P4, P5	121
Dinoflagellates	Dinophyceae	*Gymnodinium* cf. *gracilentum*	P1, P2, P4, PICE1	P4, P5, P6, P7	266
Dinoflagellates	Dinophyceae	*Gymnodinium* cf. *wulffii*	P1	P4, P5	182

(*continued on next page*)

Table A4 (*continued*)

Taxa	Class	Species	August 2018	August 2019	Carbon conversion factor (pg C cell^{-1})
Dinoflagellates	Dinophyceae	*Gymnodinium galeatum*	P1, P2, P4, PICE1	P1, P4, P5, P6, P7	266
Dinoflagellates	Dinophyceae	*Gymnodinium gracilentum*		P1	266
Dinoflagellates	Dinophyceae	*Gymnodinium ostenfeldii*		P5	57
Dinoflagellates	Dinophyceae	*Gymnodinium simplex**	P1		182
Dinoflagellates	Dinophyceae	*Gymnodinium wulffii*	P2	P4	182
Dinoflagellates	Dinophyceae	*Gyrodinium* 30–40 μm		P1	1164
Dinoflagellates	Dinophyceae	*Gyrodinium* cf. *gracilentum*		P4	266
Dinoflagellates	Dinophyceae	*Gyrodinium* cf. *wulffii*	P1		4391
Dinoflagellates	Dinophyceae	*Gyrodinium flagellare*	P1, PICE1	P1, P4, P5, P6, P7	8.0
Dinoflagellates	Dinophyceae	*Gyrodinium fusiforme*	P1, P2, PICE1	P1, P4, P5, P6, P7	2429
Dinoflagellates	Dinophyceae	*Gyrodinium grave*		P4	2567
Dinoflagellates	Dinophyceae	*Heterocapsa arctica**	P2		77
Dinoflagellates	Dinophyceae	*Heterocapsa rotundata*	P4, PICE1	P1, P4, P5, P6	36
Dinoflagellates	Dinophyceae	*Karlodinium* sp.*		P4	99
Dinoflagellates	Dinophyceae	*Katodinium glaucum*	P1, P2	P1, P4, P5, P6, P7	439
Dinoflagellates	Dinophyceae	*Lessardia elongata*	P1, PICE1	P1, P4, P5, P7	166
Dinoflagellates	Dinophyceae	*Micracanthodinium claytonii*		P4, P5, P6, P7	546
Dinoflagellates	Dinophyceae	*Oxyrrhis* sp.*	P1, P4, PICE1		45
Dinoflagellates	Dinophyceae	Peridiniales 20–30 μm		P1, P4	506
Dinoflagellates	Dinophyceae	*Phalacroma rotundatum* (formerly *Dinophysis rotundata*)		P1	2479
Dinoflagellates	Dinophyceae	*Polarella glacialis*	P1	P1, P4, P5	51
Dinoflagellates	Dinophyceae	*Pronoctiluca pelagica*		P1, P4, P6	297
Dinoflagellates	Dinophyceae	*Pronoctiluca* sp.	PICE1	P1, P5, P6, P7	297
Dinoflagellates	Dinophyceae	*Prorocentrum cordatum*	P1		173
Dinoflagellates	Dinophyceae	*Prorocentrum* sp.		P1, P5	1223
Dinoflagellates	Dinophyceae	*Protoperidinium bipes*	P1	P4	172
Dinoflagellates	Dinophyceae	*Protoperidinium brevipes*	P1, P2	P1, P6, P7	1286
Dinoflagellates	Dinophyceae	*Protoperidinium cerasus*		P1	3380
Dinoflagellates	Dinophyceae	*Protoperidinium* cf. *ovatum**	P1		5116
Dinoflagellates	Dinophyceae	*Protoperidinium depressum*	P1	P1	12,388
Dinoflagellates	Dinophyceae	*Protoperidinium pellucidum*	P1	P1, P4, P5, P6	3273
Dinoflagellates	Dinophyceae	*Protoperidinium* sp.		P5, P7	6473
Dinoflagellates	Dinophyceae	*Scrippsiella* sp.	P1	P5, P7	816
Dinoflagellates	Dinophyceae	*Tripos arcticus* (formerly *Ceratium arcticum*)	P1	P1, P4	8128
Other flagellates	Chlorodendrophyceae	*Pachysphaera pelagica*		P4	63
Other flagellates	Chlorodendrophyceae	*Pachysphaera* sp.	P1, P2	P1, P5, P6, P7	63
Other flagellates	Chlorophyceae	Chlamydomonadaceae indet.		P4	71
Other flagellates	Chlorophyceae	*Chlamydomonas* sp.		P4	71
Other flagellates	Chlorophyceae	*Dunaliella* sp.*	P2	P7	36
Other flagellates	Choanoflagellatea	*Calliacantha natans*	P1, P2	P1, P4, P5, P6, P7	39
Other flagellates	Choanoflagellatea	Choanoflagellate *indet.*	P4		5.0
Other flagellates	Choanoflagellatea	*Diaphanoeca pedicellata**		P1	21
Other flagellates	Choanoflagellatea	*Monosiga marina*	P1, P2, PICE1	P1, P4, P5, P6, P7	9
Other flagellates	Choanoflagellatea	*Pleurasiga echinocostata**		P1	5.0
Other flagellates	Choanoflagellatea	*Salpingoeca* sp.		P6, P7	10
Other flagellates	Chrysophyceae	Chrysophyceae sp.	P1, P2, PICE1	P1, P4, P5, P6, P7	77
Other flagellates	Chrysophyceae	*Dinobryon balticum*	P1, P2, P4, PICE1	P1, P4, P5, P6, P7	18
Other flagellates	Chrysophyceae	*Dinobryon divergens**	P2		32
Other flagellates	Chrysophyceae	*Dinobryon faculiferum*		P1, P4, P7	11
Other flagellates	Cryptophyceae	*Cryptomonas* sp.	P1, P2, P4, PICE1	P1, P4, P5, P6, P7	220
Other flagellates	Cryptophyceae	Cryptophyceae indet.	P2	P1, P4	34
Other flagellates	Cryptophyceae	*Hemiselmis* sp.*		P5	5
Other flagellates	Cryptophyceae	*Leucocryptos marina*	P1, P2	P1, P4, P5, P6, P7	24
Other flagellates	Cryptophyceae	*Rhodomonas* sp.		P5, P6, P7	16
Other flagellates	Cryptophyceae	*Teleaulax* sp.	P1, P2	P1, P4, P5, P6, P7	27
Other flagellates	Dictyochophyceae	*Octonaria speculum* (formerly *Dictyocha speculum*)		P1, P4, P5, P6, P7	461
Other flagellates	Eukaryota incertae sedis	Flagellates indet.	P2	P1, P4, P5, P6, P7	67
Other flagellates	Eukaryota incertae sedis	Flagellates indet. 0–3 μm	P2	P4, P6, P7	1.2
Other flagellates	Eukaryota incertae sedis	Flagellates indet. 20–30 μm		P4	205
Other flagellates	Eukaryota incertae sedis	Flagellates indet. 3–7 μm	P1, P2, P4, PICE1	P1, P4, P5, P6, P7	10

(*continued on next page*)

Table A4 (*continued*)

Taxa	Class	Species	August 2018	August 2019	Carbon conversion factor (pg C cell^{-1})
Other flagellates	Eukaryota incertae sedis	Flagellates indet. 7–10 μm	P1, P2, P4, PICE1	P1, P4, P5, P6, P7	39
Other flagellates	Prasinophyceae	*Pterosperma* sp.		P1, P4	6005
Other flagellates	Prymnesiophyceae	*Chrysochromulina* sp.	P1, P2, P4, PICE1	P1, P4, P7	38
Other flagellates	Prymnesiophyceae	Coccolithales 7–10 μm	P2		111
Other flagellates	Prymnesiophyceae	Coccolithales indet.		P1, P5	111
Other flagellates	Pyramimonadophyceae	*Phaeocystis pouchetii*	P1, P2, P4, PICE1	P1, P4, P5, P6, P7	9.4
Other flagellates	Prymnesiophyceae	*Pyramimonas* sp.	P1, P2, PICE1	P1, P4, P5, P6, P7	82
Other flagellates	Raphidophyceae	*Commation* sp.*	P2, P4	P4, P6, P7	8.0
Other flagellates	Raphidophyceae	*Heterosigma* sp.	P2	P1, P4, P5, P6, P7	242
Other flagellates	Raphidophyceae	*Olisthodiscus* sp.*	P2, P4, PICE1	P1	192
Other flagellates	Telonemea	*Telonema* sp.	P1, P4	P1, P4, P5	26
Other flagellates	Telonemea	*Telonema subtile*		P1	7.9
Ciliates	Ciliophora	Ciliophora	P2, P4, PICE1		245
Ciliates	Ciliophora	Ciliophora 10–20 μm	P1, P2, P4, PICE1		245
Ciliates	Ciliophora	Ciliophora 20–30 μm	P1, P2	P1, P5	608
Ciliates	Ciliophora	Ciliophora 30–40 μm	P1	P6	1072
Ciliates	Ciliophora	Ciliophora 50–60 μm		P1, P4	1298
Ciliates	Gymnostomatea	*Cyclotrichium* sp.*		P4	244
Ciliates	Gymnostomatea	*Didinium* sp.	P2	P4	4171
Ciliates	Gymnostomatea	*Mesodinium rubrum*	P2, P4, PICE1	P1, P4, P5, P7	3248
Ciliates	Oligohymenophorea	*Scuticociliatia indet.*		P5, P6	532
Ciliates	Oligohymenophorea	*Uronema marinum**	P1, P4		2163
Ciliates	Oligotrichea	*Acanthostomella norvegica*	P1, P2	P4, P5, P6, P7	312
Ciliates	Oligotrichea	*Laboea strobila*		P1	2711
Ciliates	Oligotrichea	*Leegaardiella ovalis*		P1	672
Ciliates	Oligotrichea	*Leegaardiella sol*	P1, P2, PICE1	P1, P4, P6, P7	456
Ciliates	Oligotrichea	*Leprotintinnus pellucidus**		P1	1660
Ciliates	Oligotrichea	*Leprotintinnus* sp.	P1		1660
Ciliates	Oligotrichea	*Lohmanniella oviformis*	P1, P2, P4, PICE1	P1, P4, P5, P6, P7	204
Ciliates	Oligotrichea	*Parafavella obtusangula*		P1	26,503
Ciliates	Oligotrichea	*Ptychocylis obtusa*	P1, P2		1660
Ciliates	Oligotrichea	*Strombidium*	P1, P2, P4, PICE1	P1, P4, P5, P7	1010
Ciliates	Oligotrichea	*Strombidium* 20–30 μm		P1, P4	779
Ciliates	Oligotrichea	*Strombidium conicum*		P1	11,170
Ciliates	Oligotrichea	*Strombidium constrictum*		P4	6377
Ciliates	Oligotrichea	Tintinnidae *indet.*	P1		1660
Ciliates	Oligotrichea	*Tintinnopsis* sp.		P5, P6, P7	1660

environment will likely change the timing of blooms, successional patterns and protist community structure (Li et al., 2009; Nöthig et al., 2015; Flores et al., 2019). In a low-ice scenario, the oligotrophic, low biomass summer season dominated by small phytoplankton as well as heterotrophic and mixotrophic protists will be prolonged and commences earlier, following an advanced spring bloom governed by an earlier sea-ice retreat. Considering the lower accessibility of small-sized protists for *Calanus* copepods, the question is how a shift in phytoplankton phenology as well as a longer oligotrophic open water season dominated by small-sized protists will impact the lipid storage capacity of the dominant copepod grazers, especially because metabolic demands are highest during the warmer summer season (Morata and Søreide, 2015). A trend towards smaller-sized algae is predicted to lengthen the food web (Vernet et al., 2019) and negatively impact the energy transfer through the classic food web leading from larger diatom-eating *Calanus* copepods (Fig. 9; Søreide et al., 2008; Campbell et al., 2009; Cleary et al., 2017) to e.g., pelagic fish. Long-term food web changes have been shown for the Northeast Atlantic as a result of an increased success of the picocyanobacteria *Synechococcus* (Schmidt et al., 2020). Besides the potential food-web impacts, a longer oligotrophic open water season dominated by small phytoplankton and hetero- and mixotrophic protists will likely also extend the period of low vertical carbon flux (Fig. 9; Wassmann and Reigstad, 2011) with unknown consequences for benthic food webs, including the northern prawn (*Pandalus borealis*) (Carroll and Carroll, 2003; Dąbrowska et al., 2020). Interestingly, the deeper mixed open-water station P1 sustained higher protist standing stocks, particularly diatoms, in late summer compared with the meltwater-stratified, previously ice-covered stations and likely shows less pronounced seasonality. This is consistent with findings from the Fram Strait that showed a reduction in the strength of the biological carbon pump as a result of sea ice-derived meltwater stratification (von Appen et al., 2021).

Funding

This work was funded by the Research Council of Norway through the project *The Nansen Legacy* (RCN # 276730).

Author Contributions

DK and PA contributed equally to the writing of the paper. Study design involved PA, RG, DK, YB, OM, MAA, GB, MR, and BE. Nutrient data were analysed by MC and EJ. KB and LMG analysed chlorophyll *a* satellite imagery. Microscopic analysis of protist community samples was carried out by AMD, AT and JMW. OM, GB and LMO contributed flow cytometry data on pico- and nanoplankton and heterotrophic

nanoflagellates. Vertical flux data was contributed by YB and MR. Data analyses and figures were done by LG with the help of the other authors. ØL provided the temperature-salinity plot (Fig. A.1). All authors contributed to data interpretation and to the writing of the manuscript.

Declaration of Competing Interest

The authors declare that they have no known competing financial interests or personal relationships that could have appeared to influence the work reported in this paper.

Data availability

Nutrient (Chierici et al., 2021a,b) and chlorophyll *a* (Vader, 2022) data have been published in the Norwegian Marine Data Centre. Phytoplankton biodiversity data (Assmy et al., 2022a,b) have been published in the Norwegian Polar Data Centre and GBIF.

Acknowledgments

The authors would like to thank the captain and the crew of *Kronprins Haakon* for their excellent support at sea during the Nansen Legacy expeditions in 2018 (JC1_2) and 2019 (Q3). We thank Tobias Vonnahme and Luka Supraha for sampling of the microbial community during the 2018 expedition, and Miriam Marquardt for support and help during the field sampling in 2019. We thank Evy Foss Skjoldal for taking flow cytometry samples during the 2018 expedition and Elzbieta Anna Petelenz for laboratory analysis of flow cytometry samples.

Appendix A

Figs. A1–A7 and Tables A1–A4.

References

Acevedo-Trejos, E., Brandt, G., Steinacher, M., Merico, A., 2014. A glimpse into the future composition of marine phytoplankton communities. Front. Mar. Sci. 1, 15.
Ardyna, M., Claustre, H., Sallée, J.B., d'Ovidio, F., Gentili, B., van Dijken, G., et al., 2017. Delineating environmental control of phytoplankton biomass and phenology in the Southern Ocean. Geophys. Res. Lett. 44, 5016–5024.
Ardyna, M., Mundy, C., Mills, M.M., Oziel, L., Grondin, P.-L., Lacour, L., et al., 2020. Environmental drivers of under-ice phytoplankton bloom dynamics in the Arctic Ocean. Elem. Sci. Anthr. 8, 30.
Arrigo, K., van Dijken, G., 2015. Continued increases in Arctic Ocean primary production. Prog. Oceanogr. 136, 60–70.
Årthun, M., Eldevik, T., Smedsrud, L.H., Skagseth, Ø., Ingvaldsen, R.B., 2012. Quantifying the influence of Atlantic heat on Barents Sea ice variability and retreat. J. Clim. 25, 4736–4743.
Årthun, M., Eldevik, T., Smedsrud, L.H., 2019. The role of Atlantic heat transport in future Arctic winter sea ice loss. J. Clim. 32, 3327–3341.
Årthun, M., Onarheim, I.H., Dörr, J., Eldevik, T., 2021. The seasonal and regional transition to an ice-free Arctic. Geophys. Res. Lett. 48, e2020GL090825.
Assmy, P., Gradinger, R., Edvardsen, B., Wold, A., Goraguer, L., Wiktor, J., Tatarek, A., 2022. Phytoplankton biodiversity Nansen Legacy JC1 [Data set]. Norwegian Polar Institute. https://doi.org/10.21334/npolar.2022.c86f931f.
Assmy, P., Gradinger, R., Edvardsen, B., Wold, A., Goraguer, L., Wiktor, J., Tatarek, A., Dąbrowska, A.M., 2022b. Phytoplankton biodiversity Nansen Legacy Q3 [Data set]. Norwegian Polar Institute. https://doi.org/10.21334/npolar.2022.dadccf78.
Assmy, P., Kvernvik, A.C., Hop, H., Hoppe, C.J.M., Chierici, M., David, T.D., Duarte, P., Fransson, A., et al., 2023. Plankton dynamics in Kongsfjorden during two years of contrasting environmental conditions. Prog. Oceanogr. 213, 102996.
Barton, A.D., Irwin, A.J., Finkel, Z.V., Stock, C.A., 2016. Anthropogenic climate change drives shift and shuffle in North Atlantic phytoplankton communities. J. Proc. Nat. Acad. Sci. 113, 2964–2969.
Blix, K., Pálffy, K., Tóth, V.R., Eltoft, T., 2018. Remote sensing of water quality parameters over Lake Balaton by using Sentinel-3 OLCI. J. Water 10, 1428.
Blondeau-Patissier, D., Gower, J.F., Dekker, A.G., Phinn, S.R., Brando, V.E., 2014. A review of ocean color remote sensing methods and statistical techniques for the detection, mapping and analysis of phytoplankton blooms in coastal and open oceans. Prog. Oceanogr. 123, 123–144.
Børsheim, K.Y., Bratbak, G., 1987. Cell volume to cell carbon conversion factors for a bacterivorous *Monas* sp. enriched from seawater. Mar. Ecol. Prog. Ser. 36, ll.
Buitenhuis, E.T., Li, W.K., Vaulot, D., Lomas, M.W., Landry, M., Partensky, F., et al., 2012. Picophytoplankton biomass distribution in the global ocean. J. Earth Syst. Sci. Data 4, 37–46.
Campbell, R.G., Sherr, E.B., Ashjian, C.J., Plourde, S., Sherr, B.F., Hill, V., Stockwell, D. A., 2009. Mesozooplankton prey preference and grazing impact in the western Arctic Ocean. Deep Sea Res II 56, 1274–1289.
Carroll, M.L., Carroll, J., 2003. The Arctic seas. In: Black, K., Shimmield, G. (Eds.), Biogeochemistry of Marine Systems. Blackwell Publishing Ltd., Oxford, pp. 127–156.
Chierici, M., Jones, E., Fransson, A., 2021a. Water column data on dissolved inorganic nutrients (nitrite, nitrate, phosphate and silicic acid) from the Nansen Legacy joint cruise KH 2018707 with *R.V.* Kronprins Haakon. https://doi.org/10.21335/NMDC-839276558.
Chierici, M., Jones, E., Hodal Lødemel, H., 2021b. Water column data on dissolved inorganic nutrients (nitrite, nitrate, phosphate and silicic acid) from the Nansen Legacy joint cruise KH 2019706 with *R.V.* Kronprins Haakon. 5-27. https://doi.org/10.21335/NMDC-1472517325.
Cleary, A.C., Søreide, J.E., Freese, D., Niehoff, B., Gabrielsen, T.M., 2017. Feeding by *Calanus glacialis* in a high arctic fjord: potential seasonal importance of alternative prey. ICES J. Mar. Sci. 74, 1937–1946.
Coello-Camba, A., Agustí, S., Holding, J., Arrieta, J.M., Duarte, C.M., 2014. Interactive effect of temperature and CO_2 increase in Arctic phytoplankton. Front. Mar. Sci. 1, 49.
Dąbrowska, A.M., Wiktor, J.M., Merchel, M., Wiktor, J.M., 2020. Planktonic protists of the eastern Nordic Seas and the Fram Strait: spatial changes related to hydrography during early summer. Front. Mar. Sci. 7, 557.
Dąbrowska, A.M., Wiktor, J.M., Wiktor Jr., J.M., Kristiansen, S., Vader, A., Gabrielsen, T., 2021. When a year is not enough: Further study of the seasonality of planktonic protist communities structure in an ice-free high Arctic fjord (Adventfjorden, West Spitsbergen). Water 13, 1990.
Dalpadado, P., Arrigo, K., Hjøllo, S., Rey, F., Ingvaldsen, R.B., Sperfeld, E., et al., 2014. Productivity in the Barents Sea-response to recent climate variability. PloS One 9, e95273.
Dalpadado, P., Arrigo, K., van Dijken, G., Skjoldal, H.R., Bagøien, E., Dolgov, A.V., et al., 2020. Climate effects on temporal and spatial dynamics of phytoplankton and zooplankton in the Barents Sea. Prog. Oceanogr. 185, 102320.
Degerlund, M., Eilertsen, H., 2010. Main species characteristics of phytoplankton spring blooms in NE Atlantic and Arctic waters (68–80 N). J. Estuar. Coasts 33, 242–269.
Dong, K., Kvile, K.Ø., Stenseth, N., Stige, L., 2020. Associations among temperature, sea ice and phytoplankton bloom dynamics in the Barents Sea. Mar. Ecol. Prog. Ser. 635, 25–36.
Downes, P.P., Goult, S.J., Woodward, E.M.S., Widdicombe, C.E., Tait, K., Dixon, J.L., et al., 2021. Phosphorus dynamics in the Barents Sea. Limnol. Oceanogr. 66, S326–S342.
Drinkwater, K.F., 2011. The influence of climate variability and change on the ecosystems of the Barents Sea and adjacent waters: review and synthesis of recent studies from the NESSAS Project. Prog. Oceanogr. 90, 47–61.
Dybwad, C., Assmy, P., Olsen, L.M., Peeken, I., Nikolopoulos, A., Krumpen, T., et al., 2021. Carbon export in the seasonal sea ice zone north of Svalbard from winter to late summer. Front. Mar. Sci. 7, 525800.
Edler, L., Elbrächter, M., 2010. The Utermöhl method for quantitative phytoplankton analysis. In: Karlson, B. (Ed.), Microscopic and Molecular Methods for Quantitative Phytoplankton Analysis. United Nations Educational, Scientific and Cultural Organization (UNESCO), Paris, pp. 13–20.
Egge, J.K., Aksnes, D.L., 1992. Silicate as regulating nutrient in phytoplankton competition. Mar. Ecol. Prog. Ser. 83, 281–289.
Ellingsen, I.H., Dalpadado, P., Slagstad, D., Loeng, H., 2008. Impact of climatic change on the biological production in the Barents Sea. Climat. Change 87, 155–175.
Engelsen, O., Hegseth, E.N., Hop, H., Hansen, E., Falk-Petersen, S., 2002. Spatial variability of chlorophyll-*a* in the Marginal Ice Zone of the Barents Sea, with relations to sea ice and oceanographic conditions. J. Mar. Syst. 35, 79–97.
Falk-Petersen, S., Hop, H., Budgell, W.P., Hegseth, E.N., Korsnes, R., Løyning, T.B., et al., 2000. Physical and ecological processes in the marginal ice zone of the northern Barents Sea during the summer melt period. J. Mar. Syst. 27, 131–159.
Fernández-Méndez, M., Olsen, L.M., Kauko, H.M., Meyer, A., Rösel, A., Merkouriadi, I., et al., 2018. Algal hot spots in a changing Arctic Ocean: Sea-ice ridges and the snow-ice interface. Front. Mar. Sci. 5, 75.
Finkel, Z.V., Beardall, J., Flynn, K.J., Quigg, A., Rees, T.A.V., Raven, J.A., 2010. Phytoplankton in a changing world: cell size and elemental stoichiometry. J. Plankton Res. 32, 119–137.
Flores, H., David, C., Ehrlich, J., Hardge, K., Kohlbach, D., Lange, B.A., et al., 2019. Sea-ice properties and nutrient concentration as drivers of the taxonomic and trophic structure of high-Arctic protist and metazoan communities. Polar Biol. 42, 1377–1395.
Furevik, T., 2001. Annual and interannual variability of Atlantic Water temperatures in the Norwegian and Barents Seas: 1980–1996. Deep Sea Res. I 48, 383–404.
Giraudeau, J., Hulot, V., Hanquiez, V., Devaux, L., Howa, H., Garlan, T., 2016. A survey of the summer coccolithophore community in the western Barents Sea. J. Mar. Syst. 158, 93–105.
Grasshoff, K., Kremling, K., Ehrhardt, M., 2009. Methods of Seawater Analysis. Wiley.
Hare, C.E., Leblanc, K., DiTullio, G.R., Kudela, R.M., Zhang, Y., Lee, P.A., et al., 2007. Consequences of increased temperature and CO_2 for phytoplankton community structure in the Bering Sea. Mar. Ecol. Prog. Ser. 352, 9–16.
Hays, G.C., Richardson, A.J., Robinson, C., 2005. Climate change and marine plankton. J. Trends Ecol. Evolut. 20, 337–344.
Hegseth, E.N., Assmy, P., Wiktor, J.M., Wiktor, J., Kristiansen, S., Leu, E., et al., 2019. Phytoplankton seasonal dynamics in Kongsfjorden, Svalbard and the adjacent shelf. In: Hop, H., Wiencke, C. (Eds.), The Ecosystem of Kongsfjorden, Svalbard. Springer, pp. 173–227.

Hegseth, E.N., Sundfjord, A., 2008. Intrusion and blooming of Atlantic phytoplankton species in the high Arctic. J. Mar. Syst. 74, 108–119.
Hillebrand, H., Dürselen, C.-D., Kirschtel, D., Pollingher, U., Zohary, T., 1999. Biovolume calculation for pelagic and benthic microalgae. J. Phycol. 35, 403–424.
Hoppe, C.J.M., Wolf, K.K., Schuback, N., Tortell, P.D., Rost, B., 2018. Compensation of ocean acidification effects in Arctic phytoplankton assemblages. Nat. Clim. Change 8, 529–533.
Holm-Hansen, O., Riemann, B., 1978. *Chlorophyll* a determination: Improvements in methodology. Oikos 30, 438–447.
Hovland, E.K., Hancke, K., Alver, M.O., Drinkwater, K., Høkedal, J., Johnsen, G., et al., 2014. Optical impact of an *Emiliania huxleyi* bloom in the frontal region of the Barents Sea. J. Mar. Syst. 130, 228–240.
Hu, C., Lee, Z., Franz, B., 2012. Chlorophyll *a* algorithms for oligotrophic oceans: a novel approach based on three-band reflectance difference. J. Geophys. Res. 117, C01011.
Hunt Jr, G., Blanchard, A.L., Boveng, P., Dalpadado, P., Drinkwater, K.F., Eisner, L., et al., 2013. The Barents and Chukchi Seas: comparison of two Arctic shelf ecosystems. J. Mar. Syst. 109, 43–68.
Ingvaldsen, R.B., Assmann, K.M., Primicerio, R., Fossheim, M., Polyakov, I.V., Dolgov, A. V., et al., 2021. Physical manifestations and ecological implications of Arctic Atlantification. Nat. Rev. Earth Environ. 2, 874–889.
Ingvaldsen, R.B., 2022. CTD data from Nansen Legacy Cruise – Joint cruise 1–2. https://doi.org/10.21335/NMDC-714672628.
Isaksen, K., Nordli, Ø., Ivanov, B., Køltzow, M.A.Ø., Aaboe, S., et al., 2022. Exceptional warming over the Barents area. Sci. Rep. 12, 9371.
Jacobson, D.M., Anderson, D.M., 1986. Thecate heterotrophic dinoflagellates: feeding behavior and mechanisms 1. J. Phycol. 22, 249–258.
Kahru, M., Lee, Z., Mitchell, B.G., Nevison, C.D., 2016. Effects of sea ice cover on satellite-detected primary production in the Arctic Ocean. Biol. Lett. 12, 20160223.
Kemp, A.E.S., Pike, J., Pearce, R.B., Lange, C.B., 2000. The "Fall dump"—a new perspective on the role of a "shade flora" in the annual cycle of diatom production and export flux. Deep Sea Res. II 47, 2129–2154.
Kiørboe, T., 2011. How zooplankton feed: mechanisms, traits and trade-offs. Biol. Rev. 86, 311–339.
Kopylov, A.I., Sazhin, A.F., Zabotkina, E.A., Romanenko, A.V., Romanova, N.D., Makarevich, P.R., Wenger, M.P., 2016. Viruses, bacteria, and heterotrophic nanoflagellates in Laptev Sea plankton. Oceanology 56, 789–798.
Kroeker, K.J., Kordas, R.L., Crim, R., Hendriks, I.E., Ramajo, L., Singh, G.S., et al., 2013. Impacts of ocean acidification on marine organisms: quantifying sensitivities and interaction with warming. Glob. Change Biol. 19, 1884–1896.
Kubiszyn, A., Piwosz, K., Wiktor Jr, J.M., Wiktor, J.M., 2014. The effect of inter-annual Atlantic water inflow variability on the planktonic protist community structure in the West Spitsbergen waters during the summer. J. Plankton Res. 36, 1190–1203.
Kubiszyn, A., Wiktor, J.M., 2016. The *Gymnodinium* and *Gyrodinium* (Dinoflagellata: Gymnodiniaceae) of the West Spitsbergen waters (1999–2010): biodiversity and morphological description of unidentified species. Polar Biol. 39, 1739–1747.
Kvernvik, A.C., Hoppe, C.J.M., Lawrenz, E., Prásil, O., Greenacre, M., Wiktor, J.M., et al., 2018. Fast reactivation of photosynthesis in arctic phytoplankton during the polar night. J. Phycol. 54, 461–470.
Levinsen, H., Turner, J.T., Nielsen, T.G., Hansen, B.W., 2000. On the trophic coupling between protists and copepods in arctic marine ecosystems. Mar. Ecol. Prog. Ser. 204, 65–77.
Lewis, K.M., Arntsen, A.E., Coupel, P., Joy-Warren, H., Lowry, K., Matsuoka, A., et al., 2019. Photoacclimation of Arctic Ocean phytoplankton to shifting light and nutrient limitation. Limnol. Oceanogr. 64, 284–301.
Li, W.K., McLaughlin, F.A., Lovejoy, C., Carmack, E.C., 2009. Smallest algae thrive as the Arctic Ocean freshens. Science 326, 539–539.
Lind, S., Ingvaldsen, R.B., Furevik, T., 2018. Arctic warming hotspot in the northern Barents Sea linked to declining sea-ice import. Nat. Clim. Change 8, 634–639.
Litchman, E., Klausmeier, C.A., Schofield, O.M., Falkowski, P.G., 2007. The role of functional traits and trade-offs in structuring phytoplankton communities: scaling from cellular to ecosystem level. Ecol. Lett. 10, 1170–1181.
Loeng, H., Drinkwater, K., 2007. An overview of the ecosystems of the Barents and Norwegian Seas and their response to climate variability. Deep Sea Res II 54, 2478–2500.
Loeng, H., Ozhigin, V., Ådlandsvik, B., 1997. Water fluxes through the Barents Sea. J. Mar. Sci. 54, 310–317.
Loeng, H., 1991. Features of the physical oceanographic conditions of the Barents Sea. Polar Res. 10, 5–18.
Lundholm, N., Hasle, G.R., 2010. *Fragilariopsis* (Bacillariophyceae) of the Northern Hemisphere–morphology, taxonomy, phylogeny and distribution, with a description of *F. pacifica* sp. nov. Phycol. 49, 438–460.
Lyon, B.R., Mock, T., 2014. Polar microalgae: new approaches towards understanding adaptations to an extreme and changing environment. Biol. 3, 56–80.
Marinov, I., Doney, S.C., Lima, I.D., 2010. Response of ocean phytoplankton community structure to climate change over the 21st century: partitioning the effects of nutrients, temperature and light. Biogeosciences 7, 3941–3959.
McKenrie, C.H., Deibel, D., Paranjape, M.A., Thompson, R.J., 1995. The marine mixotroph *Dinobryon balticum* (Chrysophyceae): Phagotrophy and survival in a cold Ocean. J. Phycol. 31, 19–24.
Menden-Deuer, S., Lessard, E., 2000. Carbon to volume relationships for dinoflagellates, diatoms, and other protist plankton. Limnol. Oceanogr. 45, 569–579.
Metfies, K., von Appen, W.-J., Kilias, E., Nicolaus, A., Nöthig, E.-M., 2016. Biogeography and photosynthetic biomass of arctic marine pico-eukaroytes during summer of the record sea ice minimum 2012. PloS One 11, e0148512.
Morán, X.A.G., López-Urrutia, Á., Calvo-Díaz, A., Li, W.K., 2010. Increasing importance of small phytoplankton in a warmer ocean. Glob. Change Biol. 16, 1137–1144.
Morata, N., Søreide, J.E., 2015. Effect of light and food on the metabolism of the Arctic copepod *Calanus glacialis*. Polar Biol. 38, 67–73.
Mullin, M.M., 1963. Some factors affecting the feeding of marine copepods of the genus *Calanus*. Limnol. Oceanogr. 8, 239–250.
Mullin, M.M., Sloan, P., Eppley, R.W., 1966. Relationship between carbon content, cell volume, and area in phytoplankton. Limnol. Oceanogr. 11, 307–311.
Neeley, A.R., Harris, L.A., Frey, K.E., 2018. Unraveling phytoplankton community dynamics in the northern Chukchi Sea under sea-ice-covered and sea-ice-free conditions. Geophys. Res. Lett. 45, 7663–7671.
Neukermans, G., Oziel, L., Babin, M., 2018. Increased intrusion of warming Atlantic water leads to rapid expansion of temperate phytoplankton in the Arctic. Glob. Change Biol. 24, 2545–2553.
Nicolaus, M., Katlein, C., Maslanik, J., Hendricks, S., 2012. Changes in Arctic sea ice result in increasing light transmittance and absorption. Geophys. Res. Lett. 39, L24501.
Nöthig, E.-M., Bracher, A., Engel, A., Metfies, K., Niehoff, B., Peeken, I., et al., 2015. Summertime plankton ecology in Fram Strait—a compilation of long-and short-term observations. Polar Res. 34, 23349.
O'Reilly, J.E., Maritorena, S., B.G. Mitchell, Siegel, D.A., Carder, K.L., Garver, S.A., et al., 2000. SeaWiFS Postlaunch Calibration and Validation Analyses, Part 3. NASA Goddard Space Flight Center.
Onarheim, I.H., Årthun, M., 2017. Toward an ice-free Barents Sea. Geophys. Res. Lett. 44, 8387–8395.
Orkney, A., Platt, T., Narayanaswamy, B.E., Kostakis, I., Bouman, H.A., 2020. Bio-optical evidence for increasing *Phaeocystis* dominance in the Barents Sea. Philos. Trans. Roy. Soc. A 378, 20190357.
Owrid, G., Socal, G., Civitarese, G., Luchetta, A., Wiktor, J., Nöthig, E.-M., et al., 2000. Spatial variability of phytoplankton, nutrients and new production estimates in the waters around Svalbard. Polar Res. 19, 155–171.
Oziel, L., Neukermans, G., Ardyna, M., Lancelot, C., Tison, J.L., Wassmann, P., et al., 2017. Role for Atlantic inflows and sea ice loss on shifting phytoplankton blooms in the Barents Sea. J. Geophys. Res. 122, 5121–5139.
Oziel, L., Sirven, J., Gascard, J.-C., 2016. The Barents Sea frontal zones and water masses variability (1980–2011). Ocean Sci. 12, 169–184.
Pančić, M., Hansen, P.J., Tammilehto, A., Lundholm, N., 2015. Resilience to temperature and pH changes in a future climate change scenario in six strains of the polar diatom *Fragilariopsis cylindrus*. Biogeosciences 12, 4235–4244.
Parsons, A.R., Bourke, R.H., Muench, R.D., Chiu, C.S., Lynch, J.F., Miller, J.H., et al., 1996. The Barents Sea polar front in summer. J. Geophys. Res. 101, 14201–14221.
Paulsen, M.L., Dore, H., Garczarek, L., Seuthe, L., Mueller, O., Sandaa, R.-A., et al., 2016. *Synechococcus* in the Atlantic gateway to the Arctic Ocean. Front. Mar. Sci. 3, 191.
Piwosz, K., Walkusz, W., Hapter, R., Wieczorek, P., Hop, H., Wiktor, J.M., 2009. Comparison of productivity and phytoplankton in a warm (Kongsfjorden) and a cold (Hornsund) Spitsbergen fjord in mid-summer 2002. Polar Biol. 32, 549–559.
Post, E., Bhatt, U.S., Bitz, C.M., Brodie, J.F., Fulton, T.L., Hebblewhite, M., et al., 2013. Ecological consequences of sea-ice decline. Science 341, 519–524.
Qu, B., Gabric, A.J., Matrai, P.A., 2006. The satellite-derived distribution of chlorophyll-*a* and its relation to ice cover, radiation and sea surface temperature in the Barents Sea. Polar Biol. 29, 196–210.
Ratkova, T.N., Wassmann, P., 2002. Seasonal variation and spatial distribution of phyto- and protozooplankton in the central Barents Sea. J. Mar. Syst. 38, 47–75.
Reigstad, M., Wassmann, P., Wexels Riser, C., Øygarden, S., Rey, F., 2002. Variations in hydrography, nutrients and chlorophyll *a* in the marginal ice-zone and the central Barents Sea. J. Mar. Syst. 38, 9–29.
Reigstad, M., 2022. CTD data from Nansen Legacy Cruise - Seasonal cruise Q3. https://doi.org/10.21335/NMDC-1107597377.
Richardson, T.L., 2019. Mechanisms and pathways of small-phytoplankton export from the surface ocean. Ann. Rev. Mar. Sci. 11, 57–74.
Rivero-Calle, S., Gnanadesikan, A., Del Castillo, C.E., Balch, W.M., Guikema, S.D., 2015. Multidecadal increase in North Atlantic coccolithophores and the potential role of rising CO_2. Science 350, 1533–1537.
Rousseau, V., Mathot, S., Lancelot, C., 1990. Calculating carbon biomass of *Phaeocystis* sp. from microscopic observations. Mar. Biol. 107, 305–314.
Rynearson, T.A., Richardson, K., Lampitt, R.S., Sieracki, M.E., Poulton, A.J., Lyngsgaard, M.M., et al., 2013. Major contribution of diatom resting spores to vertical flux in the sub-polar North Atlantic. Deep Sea Res. 82, 60–71.
Sakshaug, E., Johnsen, G.H., Kovacs, K.M., 2009. Ecosystem Barents Sea. Tapir Academic Press.
Schmidt, K., Birchill, A.J., Atkinson, A., Brewin, R.J., Clark, J.R., Hickman, A.E., et al., 2020. Increasing picocyanobacteria success in shelf waters contributes to long-term food web degradation. Glob. Change Biol. 26, 5574–5587.
Serreze, M.C., Meier, W.N., 2019. The Arctic's sea ice cover: trends, variability, predictability, and comparisons to the Antarctic. Ann. NY Acad. Sci. 1436, 36–53.
Serykh, I.V., Kostianoy, A.G., 2019. Seasonal and interannual variability of the Barents Sea temperature. Ecol. Monten. 25, 1–13.
Sherr, E.B., Sherr, B.F., Fessenden, L., 1997. Heterotrophic protists in the central Arctic Ocean. Deep Sea Res. II 44, 1665–1682.
Signorini, S.R., McClain, C.R., 2009. Environmental factors controlling the Barents Sea spring-summer phytoplankton blooms. Geophys. Res. Lett. 36, L10604.
Silkin, V., Pautova, L., Giordano, M., Kravchishina, M., Artemiev, V., 2020. Interannual variability of *Emiliania huxleyi* blooms in the Barents Sea: In situ data 2014–2018. Mar. Poll. Bull. 158, 111392.
Skagseth, Ø., Eldevik, T., Årthun, M., Asbjørnsen, H., Lien, V.S., Smedsrud, L.H., 2020. Reduced efficiency of the Barents Sea cooling machine. Nat. Clim. Change 10, 661–666.

Skogen, M.D., Olsen, A., Børsheim, K.Y., Sandø, A.B., Skjelvan, I., 2014. Modelling ocean acidification in the Nordic and Barents Seas in present and future climate. J. Mar. Syst. 131, 10–20.
Slagstad, D., Wassmann, P.F., Ellingsen, I., 2015. Physical constrains and productivity in the future Arctic Ocean. Front. Mar. Sci. 2, 85.
Smedsrud, L.H., Esau, I., Ingvaldsen, R.B., Eldevik, T., Haugan, P.M., Li, C., et al., 2013. The role of the Barents Sea in the Arctic climate system. Rev. Geophys. 51, 415–449.
Smedsrud, L.H., Muilwijk, M., Brakstad, A., Madonna, E., Lauvset, S.K., Spensberger, C., et al., 2022. Nordic Seas heat loss, Atlantic inflow, and Arctic sea ice cover over the last century. Rev. Geophys. 60, e2020RG000725.
Smyth, T., Tyrrell, T., Tarrant, B., 2004. Time series of coccolithophore activity in the Barents Sea, from twenty years of satellite imagery. Geophys. Res. Lett. 31, L11302.
Søgaard, D.H., Sorrell, B.K., Sejr, M.K., Andersen, P., Rysgaard, S., Hansen, P.J., et al., 2021. An under-ice bloom of mixotrophic haptophytes in low nutrient and freshwater-influenced Arctic waters. Sci. Rep. 11, 1–8.
Søreide, J.E., Falk-Petersen, S., Hegseth, E.N., Hop, H., Carroll, M.L., Hobson, K.A., Blachowiak-Samolyk, K., 2008. Seasonal feeding strategies of *Calanus* in the high-Arctic Svalbard region. Deep Sea Res. II 55, 2225–2244.
Stoecker, D.K., Lavrentyev, P., 2018. Mixotrophic plankton in the polar seas: a pan-arctic review. Front. Mar. Sci. 5, 292.
Sugie, K., Fujiwara, A., Nishino, S., Kameyama, S., Harada, N., 2020. Impacts of temperature, CO_2, and salinity on phytoplankton community composition in the western Arctic Ocean. Front. Mar. Sci. 6, 821.
Sundfjord, A., Assmann, K.M., Lundesgaard, Ø., Renner, A.H., Lind, S., Ingvaldsen, R.B., 2020. Suggested water mass definitions for the central and northern Barents Sea, and the adjacent Nansen Basin: Workshop Report. The Nansen Legacy Report Series 8. https://doi.org/10.7557/nlrs.5707.
Syvertsen, E.E., 1991. Ice algae in the Barents Sea: types of assemblages, origin, fate and role in the ice-edge phytoplankton bloom. Polar Res. 10, 277–287.
Szymanski, A., Gradinger, R.R., 2016. The diversity, abundance and fate of ice algae and phytoplankton in the Bering Sea. Polar Biol. 39, 309–325.
Thingstad, T.F., 2020. How trophic cascades and photic zone nutrient content interact to generate basin-scale differences in the microbial food web. ICES J. Mar. Sci. 77, 1639–1647.
Tomas, C.R., 1997. Identifying Marine Phytoplankton. Elsevier.
Tremblay, J.-É., Anderson, L.G., Matrai, P., Coupel, P., Belanger, S., Michel, C., Reigstad, M., 2015. Global and regional drivers of nutrient supply, primary production and CO_2 drawdown in the changing Arctic Ocean. Prog. Oceanogr. 139, 171–196.
Tremblay, J.-É., Gagnon, J., 2009. The effects of irradiance and nutrient supply on the productivity of Arctic waters: a perspective on climate change. In: Nihoul, J.C.J., Kostianoy, A.G. (Eds.), Influence of Climate Change on the Changing Arctic and Sub-Arctic Conditions. Springer, pp. 73–93.
Utermöhl, H., 1958. Zur Vervollkommnung der quantitativen Phytoplankton-Methodik. Internationale Vereinigung für theoretische und angewandte Limnologie: Mitteilungen 9, 1–38.
Vader, A., 2022. Chlorophyll a and phaeopigments Nansen Legacy. https://doi.org/10.21335/NMDC-1371694848.
Van Engeland T. Bagøien E., Wold A., Cannaby H.A., Majaneva S., Vader A., Rønning J., Handegard N.O., Dalpadado P., Ingvaldsen R.B., Diversity and seasonal development of large zooplankton along physical gradients in the Arctic Barents Sea. Under review in *Prog. Oceanogr.* (Special Issue Nansen Legacy Seasonality).
Vernet, M., Ellingsen, I.H., Seuthe, L., Slagstad, D., Cape, M.R., Matrai, P.A., 2019. Influence of phytoplankton advection on the productivity along the Atlantic Water Inflow to the Arctic Ocean. Front. Mar. Sci. 6, 583.
Vinje, T., 2001. Anomalies and trends of sea-ice extent and atmospheric circulation in the Nordic Seas during the period 1864–1998. J. Clim. 14, 255–267.
Vodopyanova, V., Larionov, V., Makarevich, P., Vashenko, P., Bulavina, A., 2020. Phytoplankton communities of the Barents Sea frontal zone during the early spring period. In: IOP Conference Series: Earth and Environmental Science. IOP Publishing, p. 012005.
von Appen, W.-J., Waite, A., Bergmann, M., Bienhold, C., Boebel, O., Bracher, A., et al., 2021. Sea-ice derived meltwater stratification slows the biological carbon pump: results from continuous observations. Nat. Commun. 12, 1–16.
von Quillfeldt, C.H., 2000. Common diatom species in Arctic spring blooms: their distribution and abundance. Bot. Mar. 43, 499–516.
Wang, Y., Kang, J.-H., Xiang, P., Ye, Y.-Y., Lin, H.-S., Lin, M., 2019. Phytoplankton communities and size-fractioned chlorophyll *a* in newly opened summer waters of the central Arctic Ocean. Mar. Ecol. Prog. Ser. 622, 67–82.
Wassmann, P., Reigstad, M., 2011. Future Arctic Ocean seasonal ice zones and implications for pelagic-benthic coupling. Oceanography 24, 220–231.
Wassmann, P., Reigstad, M., Haug, T., Rudels, B., Carroll, M.L., Hop, H., et al., 2006. Food webs and carbon flux in the Barents Sea. Prog. Oceanogr. 71, 232–287.
Wiedmann, I., Ceballos-Romero, E., Villa-Alfageme, M., Renner, A.H.H., Dybwad, C., van der Jagt, H., et al., 2020. Arctic observations identify phytoplankton community composition as driver of carbon flux attenuation. Geophys. Res. Lett. 47, e2020GL087465.
Wiktor, J.M., Wojciechowska, K., 2005. Differences in taxonomic composition of summer phytoplankton in two fjords of West Spitsbergen, Svalbard. Pol. Polar Res. 26, 259–268.
Winter, A., Henderiks, J., Beaufort, L., Rickaby, R.E., Brown, C.W., 2014. Poleward expansion of the coccolithophore *Emiliania huxleyi*. J. Plankton Res. 36, 316–325.
Zhang, F., He, J., Lin, L., Jin, H., 2015. Dominance of picophytoplankton in the newly open surface water of the central Arctic Ocean. Polar Biol. 38, 1081–1089.
Zhang, F., Lin, L., Gao, Y., Cao, S., He, J., 2016. Ecophysiology of picophytoplankton in different water masses of the northern Bering Sea. Polar Biol. 39, 1381–1397.
Zubkov, M.V., Burkill, P.H., Topping, J.N., 2007. Flow cytometric enumeration of DNA-stained oceanic planktonic protists. J. Plankton Res. 29, 79–86.